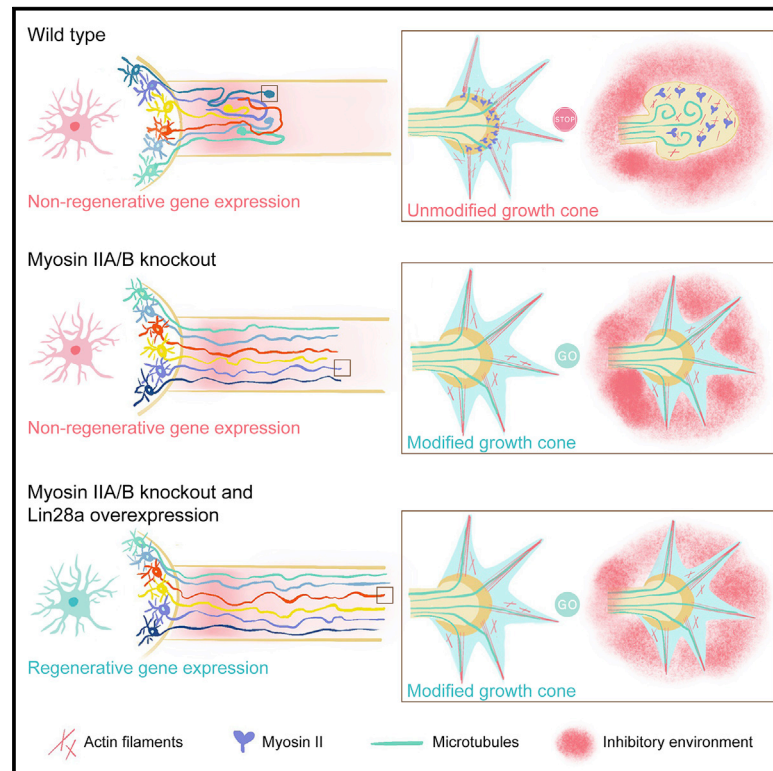


Knocking Out Non-muscle Myosin II in Retinal Ganglion Cells Promotes Long-Distance Optic Nerve Regeneration

Graphical Abstract



Authors

Xue-Wei Wang, Shu-Guang Yang, Chi Zhang, ..., Anish R. Kosanam, Saijilafu, Feng-Quan Zhou

Correspondence

saijilafu@suda.edu.cn (S.),
fzhou4@jhmi.edu (F.-Q.Z.)

In Brief

Although modulating the neuronal cytoskeleton has been deemed a promising approach to enhance mammalian axon regeneration, only a few studies have shown convincing results, especially in the central nervous system. Wang et al. demonstrate that the deletion of non-muscle myosin II sufficiently induces significant mammalian CNS axon regeneration *in vivo*.

Highlights

- Myosin II KO in RGCs induces significant optic nerve regeneration
- Myosin II KO does not affect gene transcription in RGCs
- Myosin II KO reduces retraction bulbs and leads to efficient axon extension
- Myosin II KO and Lin28a expression in RGCs produce long-distance axon regeneration



Knocking Out Non-muscle Myosin II in Retinal Ganglion Cells Promotes Long-Distance Optic Nerve Regeneration

Xue-Wei Wang,^{1,10} Shu-Guang Yang,^{1,10} Chi Zhang,^{1,3,10} Ming-Wen Hu,⁴ Jiang Qian,⁴ Jin-Jin Ma,⁵ Yingchi Zhang,¹ Bin-Bin Yang,¹ Yi-Lan Weng,⁷ Guo-Li Ming,⁸ Anish R. Kosanam,¹ Saijilafu,^{5,6,*} and Feng-Quan Zhou^{1,2,9,*}

¹Department of Orthopaedic Surgery, The Johns Hopkins University School of Medicine, Baltimore, MD 21205, USA

²The Solomon H. Snyder Department of Neuroscience, The Johns Hopkins University School of Medicine, Baltimore, MD 21205, USA

³Department of Anesthesiology and Critical Care Medicine, The Johns Hopkins University School of Medicine, Baltimore, MD 21205, USA

⁴Department of Ophthalmology, The Johns Hopkins University School of Medicine, Baltimore, MD 21205, USA

⁵Orthopaedic Institute, Medical College, Soochow University, Suzhou, Jiangsu 215007, China

⁶Department of Orthopaedic Surgery, the First Affiliated Hospital, Soochow University, Suzhou, Jiangsu 215007, China

⁷Center for Neuroregeneration, Department of Neurosurgery, Houston Methodist Research Institute, Houston, TX 77030, USA

⁸Department of Neuroscience, Perelman School of Medicine, University of Pennsylvania, Philadelphia, PA 19104, USA

⁹Lead Contact

¹⁰These authors contributed equally

*Correspondence: saijilafu@suda.edu.cn (S.), fzhou4@jhmi.edu (F.-Q.Z.)

<https://doi.org/10.1016/j.celrep.2020.107537>

SUMMARY

In addition to altered gene expression, pathological cytoskeletal dynamics in the axon are another key intrinsic barrier for axon regeneration in the central nervous system (CNS). Here, we show that knocking out myosin IIA and IIB (myosin IIA/B) in retinal ganglion cells alone, either before or after optic nerve crush, induces significant optic nerve regeneration. Combined *Lin28a* overexpression and myosin IIA/B knockout lead to an additive promoting effect and long-distance axon regeneration. Immunostaining, RNA sequencing, and western blot analyses reveal that myosin II deletion does not affect known axon regeneration signaling pathways or the expression of regeneration-associated genes. Instead, it abolishes the retraction bulb formation and significantly enhances the axon extension efficiency. The study provides clear evidence that directly targeting neuronal cytoskeleton is sufficient to induce significant CNS axon regeneration and that combining altered gene expression in the soma and modified cytoskeletal dynamics in the axon is a promising approach for long-distance CNS axon regeneration.

INTRODUCTION

Axon regeneration in the mammalian central nervous system (CNS) has been a long-standing and highly challenging issue in the biomedical research field. The current consensus is that there are two major reasons that neurons in the mature mammalian CNS do not regenerate their axons after injury. One is the hostile environment created by inhibitors in the scar tissues and degenerating myelin, and the other is the diminished intrinsic neural regeneration ability of mature CNS neurons (Curcio and

Bradke, 2018; He and Jin, 2016). Therefore, the widely accepted view is that combination strategies that target both intrinsic growth ability and inhibitory environment are likely the best option for successful CNS axon regeneration and function recovery. Early studies (David and Aguayo, 1981; Fawcett, 2018; Richardson et al., 1980; So and Aguayo, 1985) using peripheral nerve graft transplants have shown that some mature CNS neurons, such as spinal cord neurons and retinal ganglion cells (RGCs), could regenerate their axons into the permissive nerve grafts, clearly indicating that these neurons still retain limited intrinsic regeneration ability. However, to date, many studies targeting selected inhibitory molecules resulted in no or very modest CNS regeneration (Geoffroy and Zheng, 2014; Lee and Zheng, 2012). A possible reason is that there are multiple classes of inhibitory molecules, potentially including unidentified ones, which inhibit axon regeneration by distinct cellular and molecular mechanisms. Thus, targeting a few inhibitory signals while leaving the others intact may not result in a permissive environment similar to that in the peripheral nerve grafts.

In contrast, studies targeting the intrinsic axon growth ability by regulating gene expression have produced very promising results. In the optic nerve regeneration model, for example, *Pten*, *Socs3*, and *Klf4* loss of function and *Lin28* gain of function all achieved strong optic nerve regeneration (Moore et al., 2009; Park et al., 2008; Smith et al., 2009; Wang et al., 2018; Zhang et al., 2019). However, tissue clearing and 3D imaging studies revealed that many regenerating RGC axons make U-turns in the optic nerve or at the optic chiasm or make wrong guidance decisions after the chiasm (Luo et al., 2013; Pernet et al., 2013). In the corticospinal tract (CST) regeneration model, although modulation of the intrinsic regeneration ability substantially enhanced axon regeneration, most regenerating axons still cannot pass the lesion site, likely due to the effects of inhibitory molecules at the injury site. For instance, *Pten* deletion has been shown to induce, by far, the strongest promoting effect on CST axon regeneration (Liu et al., 2010). However, the most robust promoting effect can only be achieved in young mice (<1 month).



A recent study (Geoffroy et al., 2016) showed that *Pten*-deletion-induced regeneration of CST axons beyond the injury site was greatly diminished in aged mice. Specifically, in 12- to 18-month-old mice, *Pten* deletion led to little, if any, CST regeneration beyond the injury site. One potential reason for the diminished effect in older animals is the increased response to the inhibitory CNS environment. Thus, developing a successful approach for stimulating regeneration of injured CST remains a challenge, especially in older animals. A new strategy is needed to enable neurons with increased intrinsic axon growth ability to more efficiently grow axons in the inhibitory environment with fewer U-turns and to successfully cross the inhibitory boundary.

The neuronal cytoskeleton is not only the major machinery that drives axon growth (Blanquie and Bradke, 2018; Hur et al., 2011a, 2012) but also the converging targets of most, if not all, inhibitory signaling pathways (Blanquie and Bradke, 2018; Hur et al., 2012). In other words, by directly manipulating growth cone cytoskeletal motility, it is possible to interfere with how the growth cones respond to multiple inhibitory signals, regardless if these signals come from different inhibitors or function through various downstream pathways. Indeed, our previous study (Hur et al., 2011b) showed that knocking down or pharmacologically inhibiting non-muscle myosin IIA and IIB (myosin IIA/B) could allow regenerating sensory axons to grow straight and completely ignore chondroitin sulfate proteoglycans (CSPGs) and myelin-based inhibitors. The effects were much stronger than that of the Rho kinase inhibitor. Mechanistically, inhibition of myosin IIA/B resulted in a loss of lamellipodia and actin arc, which led to significantly enhanced microtubule protrusion toward the leading edge of the growth cone. As a result, the axon growth rate over permissive substrate was greatly accelerated and halted axon growth over inhibitory substrates was immediately restarted.

Here, we found that knocking out non-muscle myosin IIA/B in RGCs induced significant optic nerve regeneration. Notably, the promoting effect was unlikely to act upstream of well-known signaling mediators of optic nerve regeneration. RNA sequencing (RNA-seq) analysis of purified RGCs showed that myosin IIA/B knockout did not alter the expression of known regeneration-associated genes (RAGs), indicating local effects in the axons. In support of this finding, detailed analyses of growth cone morphology and axon trajectory revealed that myosin IIA/B deletion almost abolished the formation of retraction bulbs and significantly enhanced the axon extension efficiency in the optic nerve. Furthermore, knocking out myosin IIA/B after optic nerve injury similarly enhanced optic nerve regeneration, indicating a potential translational application. In addition, the combination of *Lin28a* overexpression, which alters the gene expression of RGCs (Wang et al., 2018), and myosin IIA/B knockout led to an additive effect in promoting optic nerve regeneration. Collectively, our study clearly demonstrated that manipulation of the neuronal cytoskeleton alone was sufficient to promote significant CNS axon regeneration *in vivo* and provided strong evidence that combining modulated gene transcription in the neuronal soma with local manipulation of the axonal cytoskeleton was a promising approach to induce long-distance CNS axon regeneration *in vivo*.

RESULTS

Double Knockout (dKO) of Non-muscle Myosin IIA/B in RGCs Led to Significant and Persistent Optic Nerve Regeneration *In Vivo*

Non-muscle myosin II consists of two essential light chains, two regulatory light chains, and two myosin II heavy chains (MHCs). There are three different isoforms of MHCs in mammalian cells, namely IIA, IIB, and IIC encoded by *Myh 9*, *10*, and *14* genes, respectively. Myosin IIA/B with MHC IIA and IIB are the major isoforms in neurons (Hur et al., 2011b). In neuronal growth cones, both myosin IIA/B are localized near the transition zone, where microtubules and actin filaments interact (Hur et al., 2011b). Our previous study (Hur et al., 2011b) has shown that pharmacological inhibition or double knockdown of myosin IIA/B in developing or regenerating sensory neurons drastically promoted sensory axon growth over two major inhibitory substrates, myelin extracts or CSPGs. Here, we tested if myosin IIA/B loss of function could also induce axon regeneration in RGCs after optic nerve injury. To knock out both myosin IIA/B in RGCs, we crossed *Myh9^{fl/fl}* and *Myh10^{fl/fl}* mice to generate *Myh9^{fl/fl}: Myh10^{fl/fl}* mice (hereafter *myosin IIA/B^{fl/fl}*) and injected AAV2-Cre into the vitreous humors of these mice. Because the *myosin IIA/B^{fl/fl}* mice were in C57Bl6/J background, wild-type C57Bl6/J mice injected with AAV2-Cre were used as a control group. Mice of both sexes were used in all experiments, and the ages of the mice were strictly matched among groups. To examine the viral vector transduction rate, immunostaining of Cre recombinase in whole-mount retinas was performed 2 weeks after the injection. The results showed that the transduction rate in RGCs was about 90% (Figures S1A and S1C). Immunostaining of retinal sections also showed a nice colocalization of Cre staining with Tuj1-positive RGCs (Figure S1B). We also injected AAV2-Cre into tdTomato Cre reporter mice to examine the efficiency of Cre-mediated gene recombination. Strong expression of tdTomato in RGCs was observed 2 weeks after AAV2-Cre injection (Figure S1D), indicating successful gene recombination. Lastly, to examine if myosin IIA/B were indeed deleted in RGCs after AAV2-Cre injection, we injected AAV2-GFP or AAV2-Cre into the left or right (counter-balanced) vitreous humors of *myosin IIA/B^{fl/fl}* mice. Two weeks later, the RGCs were dissociated, labeled with anti-CD90.2 (Thy-1.2) antibody and purified by fluorescence-activated cell sorting (FACS). Western blot analysis using the protein extracted from the purified RGCs showed that the protein levels of myosin IIA/B were depleted (Figures S2A and S2B). Immunostaining of retinal sections with the anti-myosin IIB antibody also showed significantly reduced levels of myosin IIB in RGCs (Figures S2C and S2D). Together, these results clearly demonstrated that myosin IIA/B were successfully knocked out in RGCs 2 weeks after AAV2-Cre injection.

To determine how myosin IIA/B dKO in RGCs affected optic nerve regeneration, we performed optic nerve crush (ONC) 2 weeks after the viral injection. We first assessed optic nerve regeneration 2 weeks after the ONC. The regenerating RGC axons were labeled with anterogradely transported cholera toxin subunit B (CTB) conjugated with Alexa Fluor, which was injected into the vitreous humor 2 days prior to tissue harvest

(Figure 1A). The fixed optic nerves were first tissue cleared to be transparent and then imaged with confocal microscopy. The results showed that very limited optic nerve regeneration occurred in wild-type mice injected with AAV2-Cre. In contrast, there was greatly enhanced optic nerve regeneration in the myosin IIA/B dKO condition (Figures 1A and 1B). In the majority of optic nerves, regenerating axons reached 750 μm from the crush site. To further determine if myosin IIA/B dKO led to continued axon regeneration, we assessed optic nerve regeneration 4 weeks after the ONC. We found that at 4 weeks after ONC, myosin IIA/B dKO significantly increased not only the lengths but also the number of regenerating axons. Specifically, most optic nerves had regenerating axons reaching 2,000 μm from the crush site (Figure 1B). In addition to counting axon numbers at different distances from the crush site, we also quantified the lengths of the top 5 longest regenerating axons in each optic nerve. The results showed that in the control condition, the lengths of the top 5 axons remained almost unchanged at 2 and 4 weeks, whereas the top 5 axons of myosin IIA/B dKO RGCs continued to grow from 2 to 4 weeks (Figure 1C). Both quantification results demonstrated that knocking out myosin IIA/B in RGCs led to continued optic nerve regeneration at the same speed up to 4 weeks. When the RGC survival rate was assessed, no difference was found between wild-type and myosin IIA/B dKO RGCs (Figures 1D and 1E). Collectively, these results clearly demonstrated that knocking out myosin IIA/B was sufficient to induce significant optic nerve regeneration up to at least 4 weeks after injury without affecting RGC survival.

Knocking Out Non-muscle Myosin IIA/B Acted Additively with *Lin28a* Overexpression to Promote Long-Distance Optic Nerve Regeneration

Our recent study showed that overexpression of *Lin28a* in RGCs induced substantial optic nerve regeneration by regulation of gene expression and enhanced intrinsic axon regeneration ability (Wang et al., 2018). A later study also showed that specific expression of *Lin28a* in RGCs led to significant optic nerve regeneration (Zhang et al., 2019). Therefore, we tested if combining myosin IIA/B dKO, which reshapes axonal cytoskeletal dynamics, with *Lin28a* overexpression, which alters gene expression, could have a combinatory promoting effect

on optic nerve regeneration. The result showed that both myosin IIA/B dKO and *Lin28a* overexpression alone led to significant optic nerve regeneration 2 weeks after ONC (Figures 2A and 2B). When both treatments were combined, optic nerve regeneration was greatly enhanced, with the longest axons reaching 3.5 mm from the crush site (Figures 2A and 2B). In particular, RGCs with myosin IIA/B dKO or *Lin28a* overexpression had a relatively low number of regenerating axons growing beyond 1.75 mm from the crush site. In contrast, in the combinatory treatment group, there were a significant number of regenerating axons at 3 mm and the longest axons reached up to 3.5 mm (Figures 2A and 2B). Because the dehydration process in the tissue clearing approach results in 18% shrinkage in nerve lengths (Wang et al., 2018), the real lengths of the longest regenerating axons were more than 4 mm. Indeed, in about half of the nerves in the combinatory group, the longest regenerating axons almost reached the optic chiasm 2 weeks after ONC (Figures 2A and S3). This result suggested that myosin IIA/B dKO and *Lin28a* overexpression acted additively to promote long-distance optic nerve regeneration. Similarly, we quantified the average distances of the top 5 longest regenerating axons in each nerve. The results showed that the longest regenerating axons in the combinatory group were markedly longer than those in the single-treatment groups (Figure 2C). An analysis of RGC survival revealed that the combination of myosin IIA/B and *Lin28a* overexpression did not affect RGC survival rate (Figures 2D and 2E).

Knocking Out Non-muscle Myosin IIA/B in RGCs Did Not Significantly Affect Known Optic Nerve Regeneration Signaling Pathways

In our previous study (Hur et al., 2011b), we showed that treating adult sensory neurons cultured on CSPGs with a myosin II inhibitor, blebbistatin, could induce the halted axon to regrow within minutes. Conversely, washing out blebbistatin stopped axon growth in a very short time. Such a rapid response to blebbistatin in both ways indicated that inhibition of myosin II promoted axon growth through its direct effects on the growth cone cytoskeleton without affecting signaling events in the neuronal soma. To test this idea, we examined how myosin IIA/B dKO affected two well-known pathways

Figure 1. Deletion of Myosin IIA/B in RGCs Induced Significant and Persistent Optic Nerve Regeneration

(A) Top: experimental timeline. Bottom: representative images of optic nerves showing that deletion of myosin IIA/B in RGCs produced significant axon regeneration 2 and 4 weeks after optic nerve crush. The columns on the right display magnified images of the areas in white, dashed boxes on the left, showing axons at 250, 500, 750, 1,250, and 2,000 μm distal to the crush sites. The yellow line indicates the crush sites. Yellow arrows indicate the top 3 longest axons of each nerve. Scale bar, 100 μm (50 μm for the magnified images).

(B) Quantification of optic nerve regeneration in (A) (one-way ANOVA followed by Tukey's multiple comparisons test; $p < 0.0001$ at 250, 500, 750, 1,000, 1,250, and 1,500 μm ; $p = 0.0002, 0.0071, 0.3875, \text{ and } 0.3875$ at 1,750, 2,000, 2,250, and 2,500 μm , respectively; $n = 10$ mice in 4-week wild-type (WT) group, $n = 9$ mice in other groups).

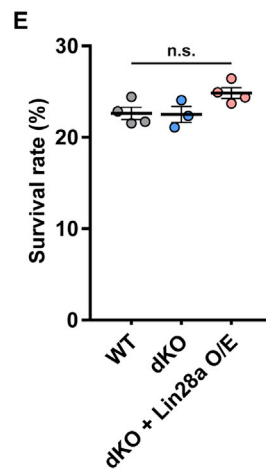
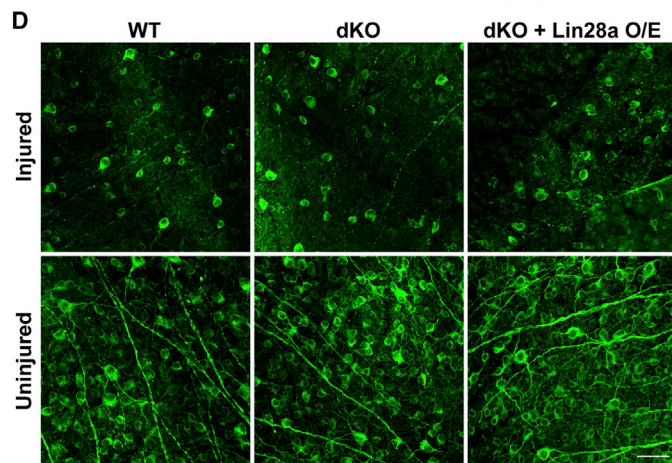
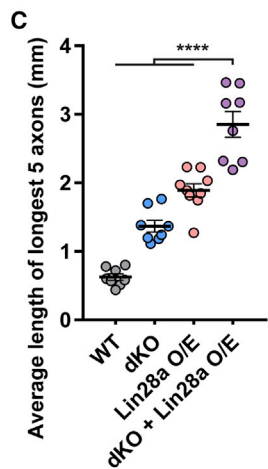
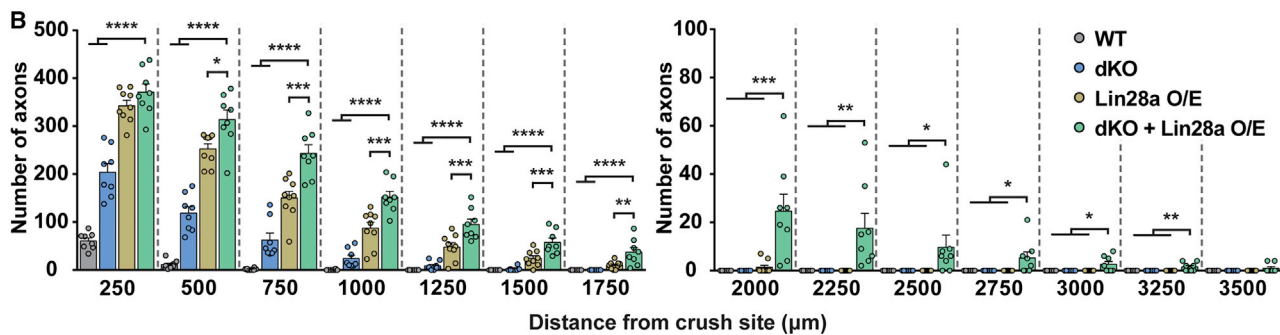
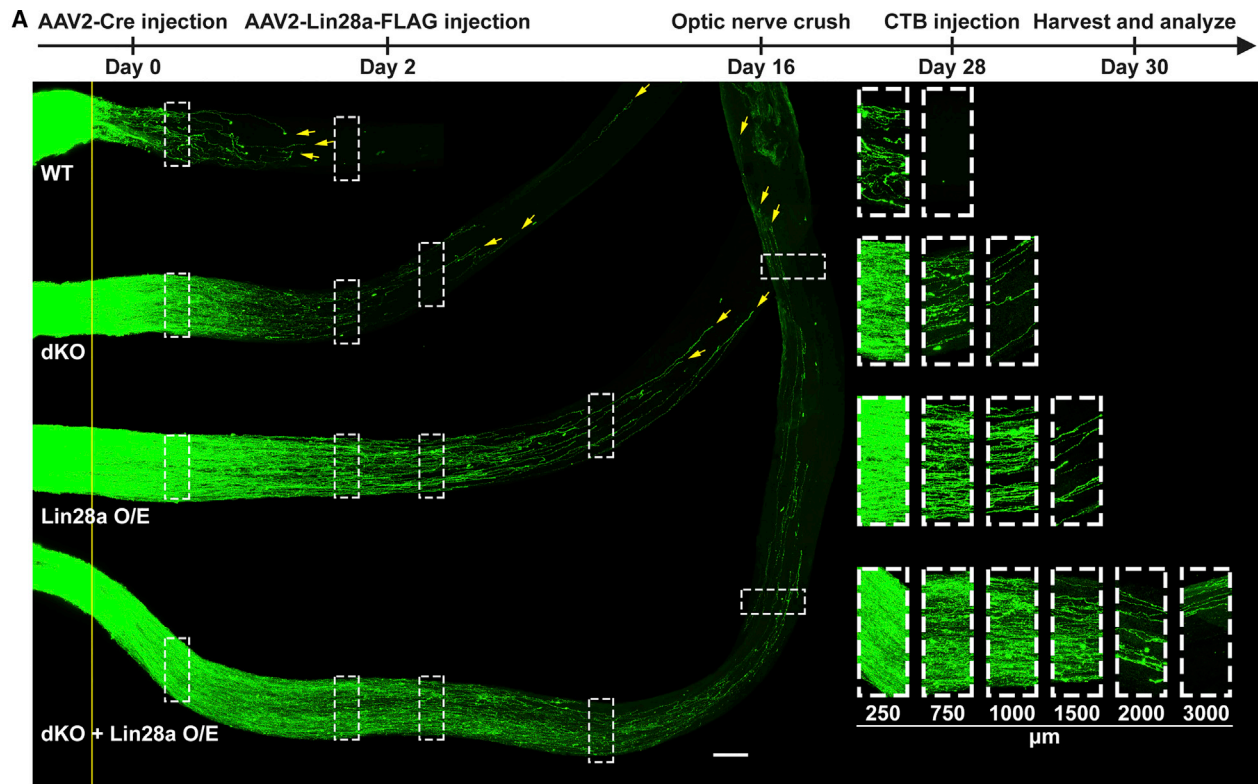
(C) Quantification of the average length of the top 5 longest axons of each nerve in (A) (one-way ANOVA followed by Tukey's multiple comparisons test; $p < 0.0001$; $n = 10$ mice in 4-week WT group, $n = 9$ mice in other groups).

(D) Representative images of flat-mounted retinas showing that deletion of myosin IIA/B had no effect on RGC survival rate 2 weeks after optic nerve crush. Flat-mounted retinas were stained with anti-tubulin $\beta 3$ antibody (Tuj1, green). Scale bar, 50 μm .

(E) Quantification of RGC survival rate in (D) (unpaired t test, $p = 0.9092$; $n = 4$ and 3 mice in WT and dKO groups, respectively; 7–8 fields were analyzed for each retina).

Data are represented as mean \pm SEM; *P* values of post hoc analyses are illustrated in the figure. n.s., not significant; * $p < 0.05$, ** $p < 0.01$, *** $p < 0.001$, **** $p < 0.0001$. dKO, double knockout of myosin IIA/B.

See also Figures S1 and S2.



(legend on next page)

governing the intrinsic axon regeneration ability, the activation of mTOR, marked by an increased level of phospho-S6 (pS6), and the inactivation of GSK3 β , marked by phosphorylation of its serine 9 residue (pGSK3 β), at 2 weeks after ONC. Previous studies have shown that most identified molecules regulating optic nerve regeneration act by either of these pathways, including *Pten* knockout (Park et al., 2008), *Akt* overexpression (Guo et al., 2016; Miao et al., 2016), *Lin28a* overexpression (Wang et al., 2018), osteopontin overexpression (Duan et al., 2015), *Socs3* deletion (Smith et al., 2009), melanopsin overexpression (Li et al., 2016), *Hdac5* manipulation (Pita-Thomas et al., 2019), and direct modulation of mTOR (Lim et al., 2016) or GSK3 β signaling (Guo et al., 2016). For mTOR activation, we examined the level of pS6 in RGCs under different conditions. The results showed that knocking out myosin IIA/B had no effect on pS6 level, whereas *Lin28a* overexpression markedly increased the level of pS6 in RGCs (Figure 3A). Quantification demonstrated that the percentage of pS6-positive (pS6 $^+$) RGCs increased by nearly 8-fold in the *Lin28a* overexpression group compared to that in the wild-type group, whereas myosin IIA/B dKO had no effect (Figure 3B). In addition, the combination of myosin IIA/B dKO and *Lin28a* overexpression did not further increase the percentage of pS6 $^+$ RGCs compared to *Lin28a* overexpression alone (Figures S4A and S4B). In comparison with our previous study (Wang et al., 2018), the higher percentage of pS6 $^+$ RGCs in the *Lin28a* overexpression condition observed here was likely caused by the fact that we performed an additional antigen retrieval step for immunohistochemistry in this study (see STAR Methods). To provide a more objective measurement of the pS6 level in RGCs, we also quantified the average fluorescence intensity of pS6 staining in all Tuj1-positive (Tuj1 $^+$) RGCs. The results showed that myosin IIA/B dKO actually slightly reduced the pS6 level compared to that of the wild-type group. In contrast, *Lin28a* overexpression greatly increased the pS6 level (Figure 3C). Lastly, we quantified the average fluorescence intensity of pS6 staining only in pS6 $^+$ RGCs under different conditions. Similarly, there was no significant difference between wild-type and myosin IIA/B dKO RGCs, whereas the *Lin28a* overexpression group had a much higher value (Figure 3D).

For GSK3 β inactivation, we found that there were very few wild-type RGCs showing positive staining of pGSK3 β and that knocking out myosin IIA/B had no impact on it (Figures 3E and 3F). In contrast, *Lin28a* overexpression increased the percentage of pGSK3 β -positive (pGSK3 β^+) RGCs by about 6-fold (Figure 3F). The average fluorescence intensity of pGSK3 β staining in all Tuj1 $^+$ RGCs was not affected by myosin IIA/B dKO, whereas *Lin28a* overexpression greatly increased the pGSK3 β level (Figure 3G). When the average fluorescence intensity of pGSK3 β was quantified only in pGSK3 β^+ RGCs, the level of pGSK3 β was decreased in the myosin IIA/B dKO group compared to that in the wild-type group, whereas the level of pGSK3 β in the *Lin28a* overexpression group was still the highest (Figure 3H).

Taken together, these results provided clear and strong evidence that knocking out myosin IIA/B did not activate the mTOR pathway or inactivate GSK3 β to support the intrinsic regenerative ability of RGCs.

Knocking Out Non-muscle Myosin IIA/B in RGCs and Peripheral Sensory Neurons Did Not Affect Known RAGs or Regeneration Pathways

To further explore the molecular mechanisms underlying the myosin-IIA/B-dKO-induced RGC axon regeneration, we performed RNA-seq in FACS-purified RGCs 2 weeks after intravitreal injection of AAV2-GFP or AAV2-Cre in *myosin IIA/B^{fl/fl}* mice. Principal-component analysis (Figure 4A), hierarchical clustering (Figure 4B), and pairwise Pearson correlations (Figure 4C) revealed that although the 6 libraries could be unquestionably clustered into 2 groups consistent to their conditions, all 6 libraries were very similar to one another, indicating RGC gene transcription was not significantly affected by myosin IIA/B dKO. In line with this, only 31 differentially expressed genes (DEGs) were identified from a total of 10,165 qualified genes (see STAR Methods) detected in the RNA-seq (Table S1). Gene Ontology (GO) analysis of these 31 genes resulted in GO terms not specifically relevant to axon growth or regeneration (Figure 4D).

Previously, we reported that double knockdown of myosin IIA/B in dorsal root ganglion (DRG) neurons drastically promoted regenerative axon growth over CSPGs or CNS myelin

Figure 2. Myosin IIA/B Deletion and *Lin28a* Overexpression Had an Additive Effect on Optic Nerve Regeneration

(A) Top: experimental timeline. Bottom: representative images of optic nerves showing that combining myosin IIA/B deletion with *Lin28a* overexpression in RGCs produced much stronger axon regeneration 2 weeks after the optic nerve crush. The columns on the right display magnified images of the areas in white, dashed boxes on the left, showing axons at 250, 750, 1,000, 1,500, 2,000, and 3,000 μ m distal to the crush sites. The yellow line indicates the crush sites. Yellow arrows indicate the top 3 longest axons of each nerve. Scale bar, 100 μ m (50 μ m for the magnified images).

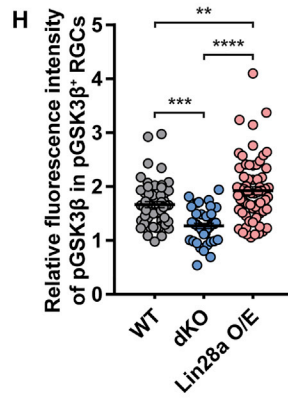
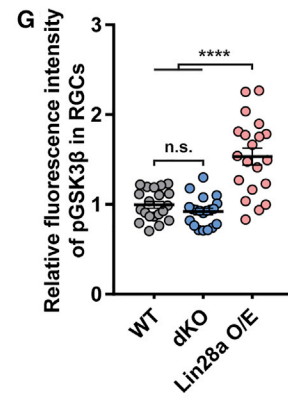
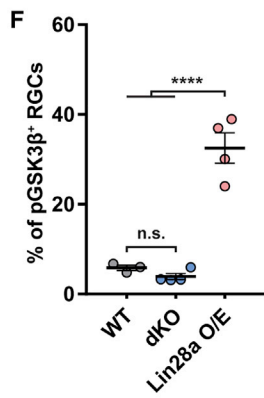
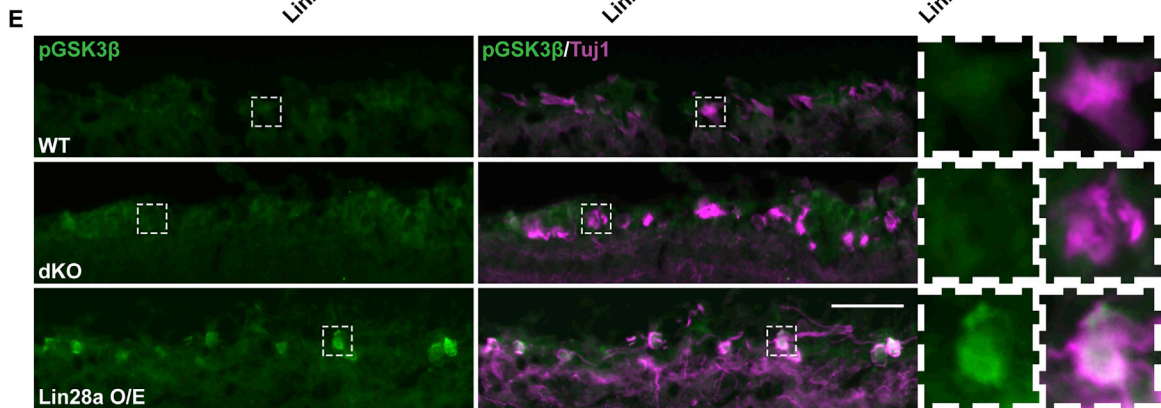
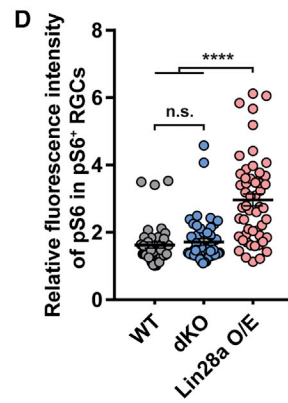
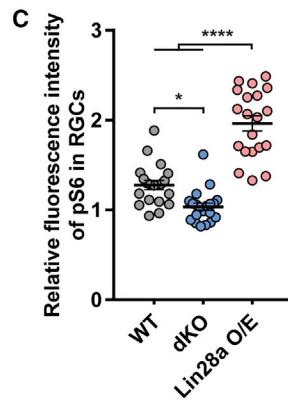
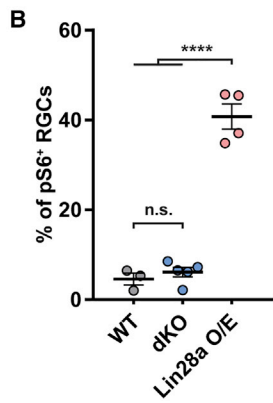
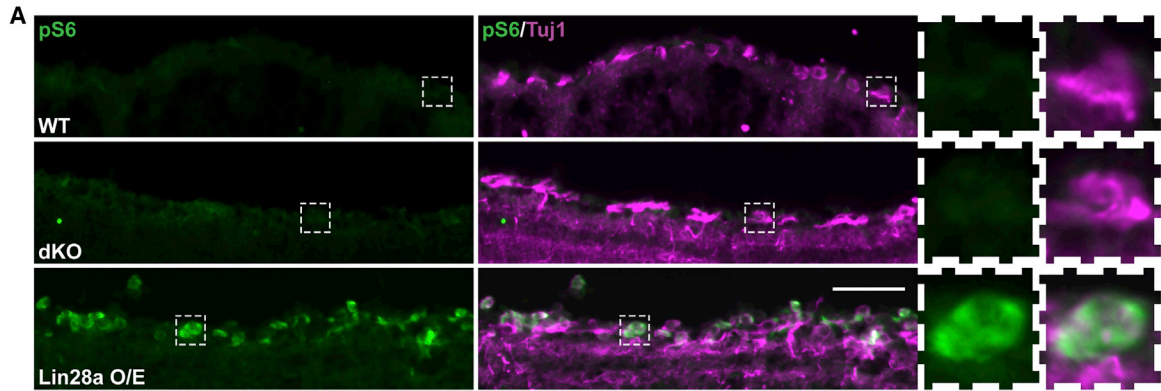
(B) Quantification of optic nerve regeneration in (A) (one-way ANOVA followed by Tukey's multiple comparisons test; $p < 0.0001$ at 250, 500, 750, 1,000, 1,250, 1,500, 1,750, and 2,000 μ m; $p = 0.0004, 0.0206, 0.0092, 0.0042, 0.0026, \text{ and } 0.0844$ at 2,250, 2,500, 2,750, 3,000, 3,250, and 3,500 μ m, respectively; $n = 9$ mice in *Lin28a* overexpression [O/E] group, $n = 8$ mice in other groups).

(C) Quantification of the average length of the top 5 longest axons of each nerve in (A) (one-way ANOVA followed by Tukey's multiple comparisons test, $p < 0.0001$; $n = 9$ mice in *Lin28a* O/E group, $n = 8$ mice in other groups).

(D) Representative images of flat-mounted retinas showing that neither myosin IIA/B deletion nor combination of myosin IIA/B deletion and *Lin28a* overexpression had any effect on RGC survival rate 2 weeks after optic nerve crush. Flat-mounted retinas were stained with anti-tubulin β 3 antibody (Tuj1, green). Scale bar, 50 μ m.

(E) Quantification of RGC survival rate in (D) (one-way ANOVA followed by Tukey's multiple comparisons test, $p = 0.0672$; $n = 3$ mice in dKO group, $n = 4$ mice in other groups; 7–8 fields were analyzed for each retina). Note that the WT and dKO groups are identical to those in Figure 1E.

Data are represented as mean \pm SEM; *P* values of post hoc analyses are illustrated in the figure. * $p < 0.05$, ** $p < 0.01$, *** $p < 0.001$, **** $p < 0.0001$. See also Figure S3.



(legend on next page)

(Hur et al., 2011b), similar to our finding in RGCs in this study. Therefore, we generated *Advillin-Cre: myosin IIA/B^{fl/fl}* mice, in which myosin IIA/B were conditionally knocked out in peripheral sensory neurons, to explore if myosin IIA/B dKO affected known RAGs and regeneration pathways in DRG neurons. We performed sham surgery or bilateral sciatic nerve injury (SNI) on these mice or *myosin IIA/B^{fl/fl}* mice. Three days later, we collected lumbar 4 and 5 DRGs and isolated mRNA and proteins for RNA-seq and western blot analyses. Pearson correlation between pairwise libraries showed that under the sham condition, the two wild-type replicates were very similar to the two dKO replicates (Figure S5A). When the numbers of DEGs were compared, we found that SNI significantly changed the mRNA levels of over 1,800 genes, whereas myosin IIA/B dKO only changed the levels of 303 genes in the absence of SNI, which was equivalent to the number of DEGs found between two biological replicates within each condition (Figure S5B). Consistent with our finding in RGCs, a GO analysis of these 303 genes revealed no specific connection with axon regeneration (Figure S5C). In addition, we closely compared the FPKMs (fragments per kilobase of transcript per million mapped reads) of many classic RAGs and genes well known to control axon regeneration, such as *Atf3*, *Sox11*, *Lin28a*, *Gap43*, *Pten*, *Klf9*, and *Rab27* (Apara et al., 2017; Christie et al., 2010; Sekine et al., 2018; Tanabe et al., 2003; Tsujino et al., 2000; Wang et al., 2018). The results showed that the mRNA levels of these genes were up- or downregulated by SNI, as expected, but were not largely affected by myosin IIA/B dKO (Figures S5D and S5E). Lastly, we directly examined the protein levels of several genes and mediators regulating axon regeneration by western blot and found that within sham or SNI condition, myosin IIA/B dKO did not change the protein levels of *Atf3*, *c-Jun*, *Gap43*, or *c-Myc* (Figures S5F and S5G). Moreover, consistent with our immunostaining results in RGCs, myosin IIA/B dKO had no impact on the mTOR (indicated by pS6) or GSK3 β pathways (Figures S5F and S5G) in DRG neurons.

Overall, these results further supported the idea that the myosin-IIA/B-dKO-induced optic nerve regeneration was unlikely to be caused by altered levels of genes or pathways related to axon regeneration.

Knocking Out Non-muscle Myosin IIA/B in RGCs Changed Axon Tip Morphology and Regenerating Axon Trajectory

To better understand the cellular mechanisms by which myosin IIA/B dKO promoted optic nerve regeneration locally at the axons, we first performed a detailed analysis of axonal tip morphology in wild-type and myosin IIA/B dKO optic nerves 2 and 4 weeks after ONC. Based on a previous study (Ertürk et al., 2007), there are mainly three types of dynamic axonal tip morphologies *in vivo*. One is the retraction bulb (Figures 5A and 5C), which is the hallmark structure of dystrophic axons that failed to regenerate (Blanquie and Bradke, 2018; Hur et al., 2012). The other two are growth-competent growth cones with two different end shapes (Figures 5A and 5C). We found that in wild-type optic nerves, a significant percentage of axons had retraction bulbs at their ends, whereas knocking out myosin IIA/B in RGCs almost completely abolished the formation of retraction bulbs (Figures 5A and 5B). Most regenerating axons in the myosin IIA/B dKO nerves had growth-competent growth cones, indicating that deleting myosin IIA/B efficiently transformed dystrophic axon tips into growth cones and rendered subsequent axon regeneration.

The tissue clearing and confocal imaging of whole-mount optic nerves allowed us to visualize the bona fide morphology of regenerating axons. Thus, we next examined how myosin IIA/B dKO influenced the axon extension trajectory 4 weeks after ONC. We analyzed the axon extension efficiency and U-turn rate for each optic nerve. For each nerve, the axon extension efficiency was calculated by dividing the summed displacement by the summed covered distance of axons (see Figure 5F and STAR Methods), and the U-turn rate represented the percentage

Figure 3. Myosin-IIA/B-Deletion-Induced Optic Nerve Regeneration Was Not Mediated by mTOR or GSK3 β Pathway

- (A) Representative images of retinal sections showing that the deletion of myosin IIA/B did not activate mTOR (marked by pS6) in RGCs, whereas *Lin28a* overexpression markedly activated mTOR in RGCs 2 weeks after optic nerve crush. The two columns on the right display magnified images of the RGCs marked in white, dashed boxes on the left. Retinal sections were stained with anti-pS6 (green) and anti-tubulin β 3 (magenta) antibodies. Scale bar, 50 μ m (12.5 μ m for the magnified images).
- (B) Quantification of the percentage of pS6⁺ RGCs in (A) (one-way ANOVA followed by Tukey's multiple comparisons test, $p < 0.0001$; $n = 3$ mice in WT group, $n = 5$ mice in dKO group, $n = 4$ mice in *Lin28a* O/E group; at least 363 RGCs from at least 7 non-adjacent retinal sections were analyzed for each mouse).
- (C) Quantification of average fluorescence intensity of pS6 in all RGCs (one-way ANOVA followed by Tukey's multiple comparisons test, $p < 0.0001$; $n = 20$ retinal sections with identical imaging configurations from at least 2 mice were analyzed for each group).
- (D) Quantification of average fluorescence intensity of pS6 in pS6⁺ RGCs (one-way ANOVA followed by Tukey's multiple comparisons test, $p < 0.0001$; $n = 42$, 49, and 53 RGCs with identical imaging configurations from at least 2 mice were analyzed for WT, dKO, and *Lin28a* O/E groups, respectively).
- (E) Representative images of retinal sections showing that the deletion of myosin IIA/B did not inactivate GSK3 β (marked by pGSK3 β) in RGCs, whereas *Lin28a* overexpression markedly inactivated GSK3 β in RGCs 2 weeks after optic nerve crush. The right two columns display magnified images of the RGCs marked in white, dashed boxes on the left. Retinal sections were stained with anti-pGSK3 β (green) and anti-tubulin β 3 (magenta) antibodies. Scale bar, 50 μ m (12.5 μ m for the magnified images).
- (F) Quantification of the percentage of pGSK3 β ⁺ RGCs in (E) (one-way ANOVA followed by Tukey's multiple comparisons test, $p < 0.0001$; $n = 3$ mice in WT group, $n = 4$ mice in other groups; at least 434 RGCs from at least 7 non-adjacent retinal sections were analyzed for each mouse).
- (G) Quantification of average fluorescence intensity of pGSK3 β in all RGCs (one-way ANOVA followed by Tukey's multiple comparisons test, $p < 0.0001$; $n = 20$ retinal sections with identical imaging configurations from at least 2 mice were analyzed for each group).
- (H) Quantification of average fluorescence intensity of pGSK3 β in pGSK3 β ⁺ RGCs (one-way ANOVA followed by Tukey's multiple comparisons test, $p < 0.0001$; $n = 54$, 40, and 65 RGCs with identical imaging configurations from at least 2 mice were analyzed for WT, dKO, and *Lin28a* O/E groups, respectively). Data are represented as mean \pm SEM; *P* values of post hoc analyses are illustrated in the figure. * $p < 0.05$, ** $p < 0.01$, *** $p < 0.001$, **** $p < 0.0001$. See also Figure S4.

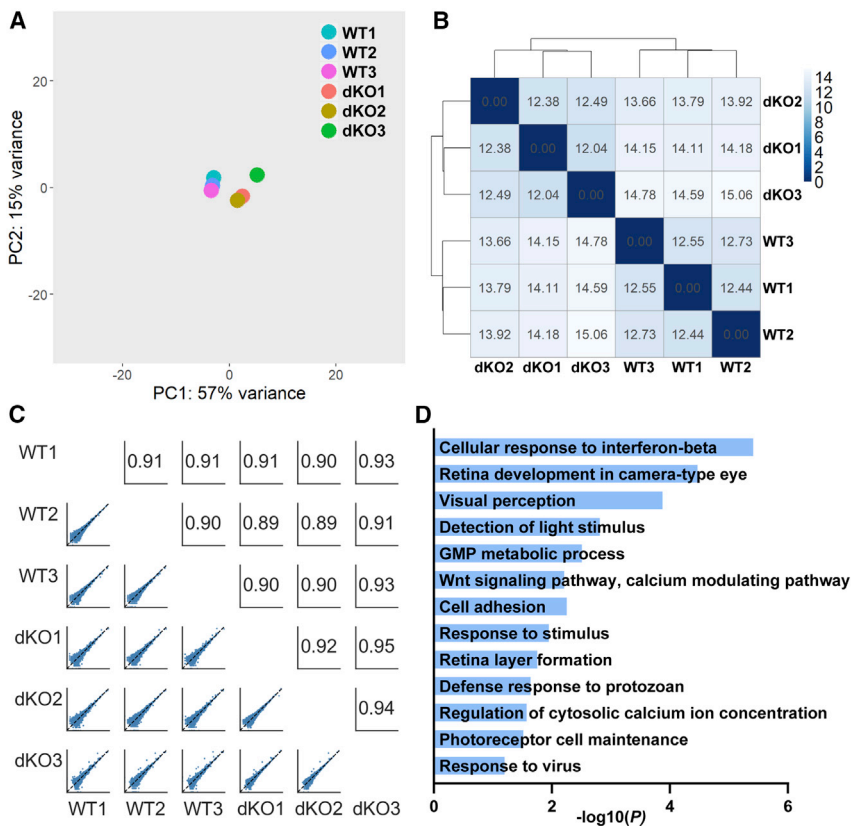


Figure 4. Myosin IIA/B Deletion Did Not Significantly Affect General Gene Transcription in RGCs

(A) Principal-component analysis of RNA-seq libraries of purified RGCs showing the high degree of similarity in gene transcription between WT and myosin-IIA/B-deleted RGCs.

(B) Hierarchical clustering of RNA-seq libraries showing the similarity in transcriptome between WT and myosin-IIA/B-deleted RGCs. The value in each grid represents the Euclidean distance between two libraries.

(C) Pairwise correlations of RNA-seq libraries showing that the myosin IIA/B deletion had little impact on gene transcription of RGCs. The lower left shows the scattered plots of normalized counts between pairwise libraries. The upper right shows the Pearson correlation coefficient between pairwise libraries.

(D) Gene Ontology analysis of differentially expressed genes between WT and myosin-IIA/B-deleted RGCs showing that myosin IIA/B deletion did not affect axon regeneration related gene transcription in RGCs.

See also [Figure S5](#) and [Table S1](#).

of axons that made a U-turn near their axonal tips. In wild-type nerves, the majority of axons followed a wandering path with many curves and U-turns, resulting in very inefficient axon regeneration toward the distal optic nerve. In contrast, in myosin IIA/B dKO nerves, most regenerating axons were straight with significantly reduced U-turns ([Figures 5D–5F](#), [S6](#), and [S7](#)), indicating a higher efficiency of axon regeneration toward the distal end. To better show the differences in axon tip morphology and axon trajectory between wild-type and myosin IIA/B dKO RGCs, we created a 3D animation of an optic nerve in each condition ([Videos S1](#) and [S2](#)).

Together, we think that the enhanced optic nerve regeneration induced by myosin IIA/B dKO was likely achieved through (1) switching retraction bulbs into growth-competent growth cones and (2) more efficient axon regeneration with straighter axon growth and less U-turns.

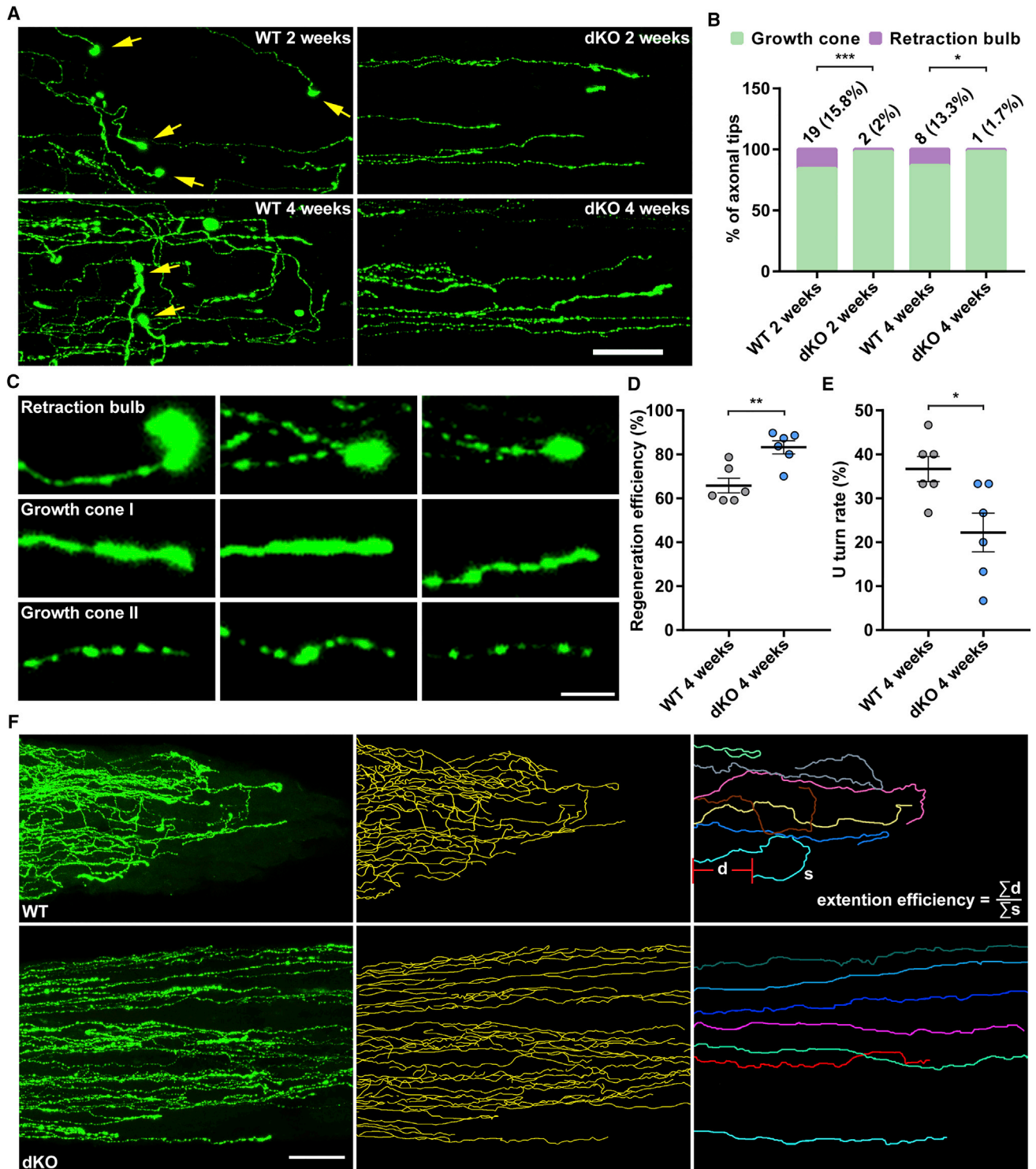
Knocking Out Non-muscle Myosin IIA/B in RGCs after ONC Could Also Induce Optic Nerve Regeneration

To investigate the translational potentials of myosin IIA/B dKO, we tested if post-injury deletion of myosin IIA/B in RGCs could also promote axon regeneration. We first performed the ONC on wild-type and *myosin IIA/B*^{fl/fl} mice, and 1 day after that, we injected AAV2-Cre into the vitreous humors of these mice. The optic nerve regeneration was assessed 3 weeks after the ONC ([Figure 6A](#)). The result showed that only a small number of axons regenerated for a limited distance in the wild-type optic

nerves. In contrast, a large number of regenerating axons were observed in dKO optic nerves ([Figure 6B](#)). Most myosin IIA/B dKO optic nerves had regenerating axons reaching 1,500 μm from the crush site, although the most noticeable difference between the two groups was found at 500–1,250 μm from the crush site ([Figure 6B](#)). Such a result clearly demonstrated that post-injury treatment with myosin IIA/B dKO could successfully induce axon regeneration in injured optic nerves, indicating that myosin IIA/B dKO may potentially be applied to translational practices in treating diseases and injuries involving axon damage.

DISCUSSION

In addition to the diminished intrinsic axon regeneration capacity regulated by changes in gene expression during neuronal maturation, the dystrophic growth cone with disruptive cytoskeletal dynamics is another key intrinsic barrier for successful CNS axon regeneration ([Blanquie and Bradke, 2018](#)). Although it has been well recognized that modulation of the axonal cytoskeleton would be a plausible approach to enhance CNS axon regeneration, very few studies have shown direct and convincing results. Previously, two elegant studies ([Hella et al., 2011](#); [Ruschel et al., 2015](#)) have shown that moderate stabilization of microtubules with taxol or epothilone B could promote axon regeneration after spinal cord injury. The promoting effects were achieved through decreased fibrotic scar formation, which rendered the lesion site more permissive, and improved microtubule protrusion in the growth cones of the injured axons. However, the promoting effects were moderate, with regenerating axons only entering the injury site. Similarly, low dose taxol



(legend continued on next page)

treatment alone after optic nerve injury had little promoting effects on axon regeneration (Sengottuvel et al., 2011). Recently, a study by Tedeschi et al. (2019) demonstrated that actin depolymerizing factor and cofilin-mediated actin turnover were both necessary and sufficient for sensory axon regeneration in the spinal cord.

In this study, we provided clear evidence that knocking out myosin IIA/B in RGCs alone was sufficient to induce significant optic nerve regeneration. Our previous *in vitro* study (Hur et al., 2011b) demonstrated that deleting myosin IIA/B acted locally at the growth cone without affecting signaling events at the neuronal soma or gene transcription. Specifically, we showed that inhibiting myosin II activity resulted in a reduced level of actin filaments in the growth cone. The retrograde flow of F-actin driven by myosin II acts as a dynamic barrier for microtubule protrusion in the growth cone. As a result, inhibition of myosin II led to significant microtubule protrusion toward the leading edge of the growth cone and increased axon growth rate. Moreover, the promoting effect of myosin II inhibition over inhibitory substrates (CSPGs) occurred within minutes and was reversible, further supporting the conclusion that the effect was local. Indeed, here, we carefully examined how RGC axonal morphology and trajectory were affected by myosin IIA/B dKO. The inability of mature CNS axon to form a growth-competent growth cone in the inhibitory environment after injury is a hallmark of regeneration failure (Blanquie and Bradke, 2018; Hur et al., 2012). In most cases, after CNS injuries, a bulb-like structure is formed at the tip of injured axons, called the retraction bulb (Ertürk et al., 2007). In wild-type mice, very limited optic nerve regeneration was observed, and retraction bulbs were more often observed at the tips of the axons. In contrast, in myosin IIA/B dKO nerves, very few retraction bulbs were identified, whereas growth-competent growth cones could be found at most axonal tips. The results indicated that deleting myosin IIA/B was an efficient strategy to transform retraction bulbs into growth cones, likely achieved through slowed retrograde flow of actin filaments and the subsequent protrusion of microtubules in the dystrophic growth cones. In addition, we found that in the wild-type group, the majority of axons had wandering trajectories with many kinks and U-turns, likely due to the inhibitory substrates in the optic nerve. Such an axon extension resulted in very inefficient axon regeneration. When myosin IIA/B were knocked out, most axons followed a straighter path with reduced U-turns, indicating myosin IIA/B deletion could overcome inhibitory cues and greatly enhance regeneration efficiency.

We also examined two well-known signaling pathways in RGCs, mTOR activation and GSK3 β inactivation, which occur in the neuronal soma to support the intrinsic axon regeneration

ability. The results showed that deleting myosin IIA/B had no effects on these two pathways, suggesting that the intrinsic axon regeneration ability of RGCs regulated by gene expression might not be altered. Next, by RNA-seq experiments using FACS-purified RGCs or DRG tissues, we showed that deleting myosin IIA/B did not significantly change the transcription profile in neurons. More importantly, the transcription levels of many known RAGs were not affected by myosin IIA/B dKO. Lastly, by western blot, we found myosin IIA/B dKO had little effect on selected RAGs and signaling mediators. Collectively, these results suggested that rather than reshaping gene expression and mediating RAGs and regeneration pathways, myosin IIA/B deletion effectively transformed retraction bulbs into active growth cones and increased axon extension efficiency to promote axon regeneration.

Long-distance axon regeneration is one of the most important aspects and is sometimes a prerequisite for successful functional recovery after neural injuries. Several previous studies (de Lima et al., 2012; Kurimoto et al., 2010; Sun et al., 2011), including ours (Wang et al., 2018), have shown that combined manipulations of multiple genes and pathways usually had additive or synergistic promoting effects on optic nerve regeneration. Given sufficient time, some axons could even regrow back to their targets in the brain and lead to partial function recovery (de Lima et al., 2012). Here, we showed that combining myosin IIA/B dKO with *Lin28a* overexpression resulted in long-distance optic nerve regeneration. Two weeks after ONC, some regenerating axons reached up to 3.25 mm from the crush site (nearly 4 mm in real distance considering 18% shrinkage due to the tissue clearing process [Wang et al., 2018]). The longest few regenerating axons were about 4.3 mm and were close to the optic chiasm. To our knowledge, such a distance of regeneration in 2 weeks after ONC was almost comparable with those in most previous studies using combinatory approaches. For instance, double knockout of *Pten* and *Socs3*, together with CNTF (ciliary neurotrophic factor) administration, led to optic nerve regeneration up to 3 mm from the crush site 2 weeks after ONC (Sun et al., 2011). Similarly, a combination of Zymosan, cyclic AMP (cAMP), and *Pten* deletion could promote optic nerve regeneration to 3 mm from the crush site in 2 weeks (Kurimoto et al., 2010). However, compared with these studies, the number of long-distance regenerating axons we observed was relatively low, which was likely due to the poor survival of RGCs in our study. It is worth noting that several factors may have contributed to the seemingly higher level of RGC axon regeneration after *Lin28a* overexpression in this study than in our previous study (Wang et al., 2018). First, in the current study, instead of using an estimated number of axons to indicate RGC axon regeneration, we used the actual number of axons in each optic nerve

(D) Quantification of axon extension efficiency in (F) (unpaired t test, $p = 0.0032$; $n = 6$ mice in each group; at least 35 axons were analyzed for each mouse).

(E) Quantification of U-turn rate in Figure S7 (unpaired t test, $p = 0.0210$; $n = 6$ mice in each group; top 15 longest axons were analyzed for each mouse).

(F) Left: representative images of optic nerves showing that the deletion of myosin IIA/B in RGCs improved axon extension efficiency 4 weeks after optic nerve crush. Middle: sketches of all axon traces in the left column. Right: detailed trajectories of a few axons (each color represents a single axon) in the left column. As illustrated, the extension efficiency of each nerve was calculated by dividing the summed displacement by the summed length of all traced axons. Scale bar, 50 μ m.

Data are represented as mean \pm SEM. * $p < 0.05$, ** $p < 0.01$, *** $p < 0.001$.

See also Figures S6 and S7 and Videos S1 and S2.

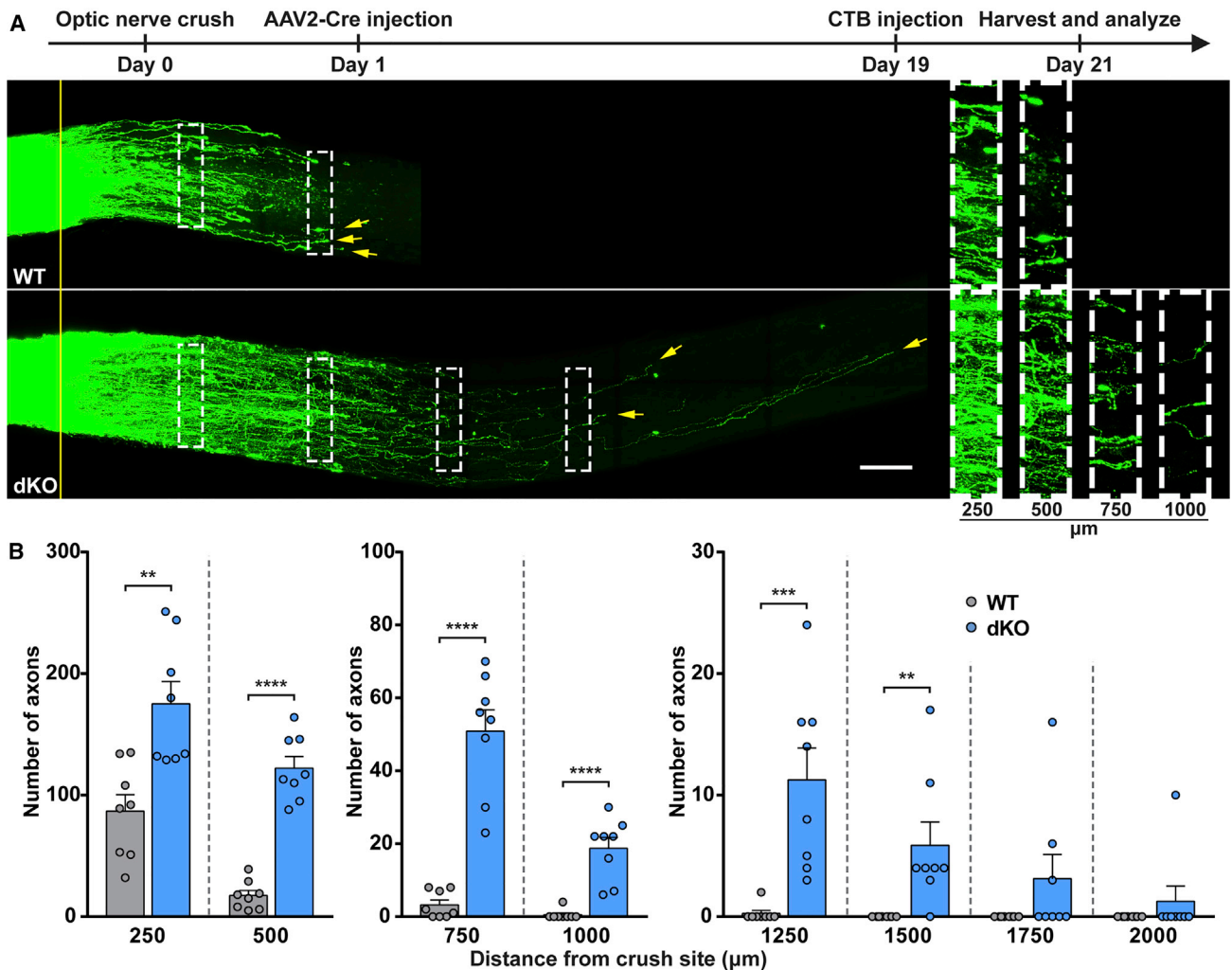


Figure 6. Post-injury Deletion of Myosin IIA/B Could Also Induce Optic Nerve Regeneration

(A) Top: experimental timeline. Bottom: representative images of optic nerves showing that post-injury deletion of myosin IIA/B in RGCs induced axon regeneration 3 weeks after optic nerve crush. The columns on the right display magnified images of the areas in white, dashed boxes; on the left, showing axons at 250, 500, 750, and 1,000 μm distal to the crush sites. The yellow line indicates the crush sites. Yellow arrows indicate the top 3 longest axons of each nerve. Scale bar, 100 μm (50 μm for the magnified images).

(B) Quantification of optic nerve regeneration in (A) (unpaired t test; $p = 0.0017$ at 250 μm ; $p < 0.0001$ at 500, 750, and 1,000 μm ; $p = 0.0009$, 0.0085, 0.1396, and 0.3343 at 1,250, 1,500, 1,750, and 2,000 μm , respectively; $n = 8$ mice in each group).

Data are represented as mean \pm SEM. ** $p < 0.01$, *** $p < 0.001$, **** $p < 0.0001$.

(see STAR Methods), and therefore, the axon numbers shown in the y axis cannot be directly compared between the two studies. Second, the optic nerve images in this study were acquired with a Zeiss LSM 800 confocal microscope, whereas those in the previous study were taken with a Zeiss LSM 510 confocal microscope. The new equipment generated images with higher quality and enabled us to detect some sparse regenerating axons far from the crush site. Last, the independently packaged AAV2-Lin28a-FLAG used in each study may also contribute to the differences. The effectiveness of the combinatory approach would be optimal if each manipulated gene and pathway could act independently. Our previous study found that *Lin28a* overexpression could induce optic nerve regeneration by modifying

gene expression and enhancing the intrinsic growth ability of RGCs (Wang et al., 2018). A recent study (Zhang et al., 2019) confirmed that specific expression of *Lin28a* in RGCs could lead to significant optic nerve regeneration. In addition, it also revealed that apart from its direct effect on RGCs, *Lin28a* specifically expressed in amacrine cells could enhance the Igf1-induced optic nerve regeneration by suppressing hyperactivity of amacrine cells induced by optic nerve injury and increasing the responsiveness of RGCs to Igf1 stimulation. As such, *Lin28a* and myosin II could act in distinct neuronal compartments with diverse cellular mechanisms, resulting in a powerful combination. Based on our RNA-seq results that only few DEGs were found between wild-type and myosin IIA/B dKO

RGCs and axon regeneration-related gene transcription was barely affected in RGCs by myosin IIA/B dKO, it is likely that the effect was mainly RGC autonomous because more transcriptional changes would be expected in RGCs if the axon regeneration was secondary to intercellular signaling. However, the current study does not have direct evidence to prove that the myosin IIA/B knockout-induced axon regeneration was RGC autonomous and, therefore, cannot completely rule out the possibility that myosin IIA/B deletion in other cell types somehow contributed to the observed results. Regardless, myosin II knockout can be a new effective option for combination strategies, and future studies combining myosin II knockout with other regeneration approaches, as well as enhanced RGC survival, may potentially lead to large number of axons regenerating back to their original targets in the brain and gain recovery of lost visual function.

Here, we also showed that deleting myosin IIA/B in RGCs after optic nerve injury could induce significant optic nerve regeneration, indicating that myosin IIA/B deletion or inhibition has the potential to be practically used in the treatment of nerve injury. Because deleting myosin IIA/B in RGCs remodels the cytoskeletal structures at the growing axonal ends, it is likely that regenerating RGC axons would not respond to guidance cues properly. In our previous *in vitro* study (Hur et al., 2011b), after blebbistatin withdrawal, the axons quickly restored their ability to respond to the CSPGs. Thus, future studies using small-molecule inhibitors would not only enhance optic nerve regeneration but also allow proper axon guidance if needed. As a result, the development of water soluble, stable, and specific pharmacological inhibitors of myosin II, such as the blebbistatin derivative (Várkuti et al., 2016), would make future translational applications possible to repair axonal injuries induced by glaucoma, spinal cord injury, traumatic brain injury, and neurodegenerative diseases.

STAR★METHODS

Detailed methods are provided in the online version of this paper and include the following:

- **KEY RESOURCES TABLE**
- **RESOURCE AVAILABILITY**
 - Lead Contact
 - Materials Availability
 - Data and Code Availability
- **EXPERIMENTAL MODEL AND SUBJECT DETAILS**
 - Mice
- **METHOD DETAILS**
 - Construct
 - Optic Nerve Regeneration Model
 - Optic Nerve Tissue Clearing
 - Analysis of RGC Axon Regeneration
 - Immunohistochemistry of Whole-Mount Retinas
 - Analysis of RGC Transduction Rate
 - Analysis of RGC Survival Rate
 - Immunohistochemistry of Retinal Sections
 - Analysis of Myosin IIB Level in RGCs
 - Analysis of S6 and GSK3 β Phosphorylation

- Sciatic Nerve Injury Model
- RGC Purification
- RGC RNA Sequencing and Data Analysis
- DRG mRNA Sequencing and Data Analysis
- Western Blot Analysis
- Analysis of Axonal Tip Morphology
- Analysis of Axon Extension Efficiency
- Analysis of U-turn Rate

● QUANTIFICATION AND STATISTICAL ANALYSIS

SUPPLEMENTAL INFORMATION

Supplemental Information can be found online at <https://doi.org/10.1016/j.celrep.2020.107537>.

ACKNOWLEDGMENTS

We acknowledge Dr. Michele Pucak from the Multiphoton Imaging Core (supported by NS050274) of the Department of Neuroscience, Johns Hopkins School of Medicine for her help in confocal microscopy. We thank Hao Zhang from the Flow Cytometry Cell Sorting Core Facility at Bloomberg School of Public Health, Johns Hopkins University for doing FACS sorting. The facility was supported by 1S100D016315-01 and 1S10RR13777001 and, in part, by CFAR: 5P30AI094189-04 (Chaisson). We appreciate the Johns Hopkins Transcriptomics and Deep Sequencing Core for doing the RGC RNA-seq experiment. We also thank Ying Zhang for drawing the graphical abstract. The study was supported by grants (to F.-Q.Z. and J.Q.) from NIH (R01NS064288, R01NS085176, R01GM111514, R01EY027347, and R01EY029548), the Craig H. Neilsen Foundation (259450), and the BrightFocus Foundation (G2017037). S. was supported by the grants from the National Natural Science Foundation of China (81571189 and 81772353), the National Key Research and Development Program (2016YFC1100203), and Innovation and Entrepreneurship Program of Jiangsu Province.

AUTHOR CONTRIBUTIONS

X.-W.W., S.-G.Y., S., and F.-Q.Z. conceived the study and designed the project; X.-W.W. and S.-G.Y. performed most of the experiments; X.-W.W. and C.Z. performed and analyzed the immunostaining and western blot experiments; M.-W.H. and J.Q. analyzed the RGC RNA-seq data; Y.Z. analyzed optic nerve regeneration; C.Z. and Y.Z. analyzed the axon morphologies and trajectories; J.-J.M. performed the DRG RNA-seq experiment; Y.-L.W. and G.-L.M. helped with the optic nerve regeneration experiments; B.-B.Y. and A.R.K. helped with the data analyses; X.-W.W. and F.-Q.Z. wrote the manuscript with contributions from all authors.

DECLARATION OF INTERESTS

The authors declare no competing financial interests.

Received: September 11, 2019

Revised: March 3, 2020

Accepted: March 30, 2020

Published: April 21, 2020

REFERENCES

- Apara, A., Galvao, J., Wang, Y., Blackmore, M., Trillo, A., Iwao, K., Brown, D.P., Jr., Fernandes, K.A., Huang, A., Nguyen, T., et al. (2017). KLF9 and JNK3 Interact to Suppress Axon Regeneration in the Adult CNS. *J. Neurosci.* *37*, 9632–9644.
- Benjamini, Y., and Hochberg, Y. (1995). Controlling the False Discovery Rate—a Practical and Powerful Approach to Multiple Testing. *J. R. Stat. Soc. B* *57*, 289–300.

- Benjamini, Y., and Yekutieli, D. (2001). The control of the false discovery rate in multiple testing under dependency. *Ann. Stat.* *29*, 1165–1188.
- Blanquie, O., and Bradke, F. (2018). Cytoskeleton dynamics in axon regeneration. *Curr. Opin. Neurobiol.* *51*, 60–69.
- Christie, K.J., Webber, C.A., Martinez, J.A., Singh, B., and Zochodne, D.W. (2010). PTEN inhibition to facilitate intrinsic regenerative outgrowth of adult peripheral axons. *J. Neurosci.* *30*, 9306–9315.
- Curcio, M., and Bradke, F. (2018). Axon Regeneration in the Central Nervous System: Facing the Challenges from the Inside. *Annu. Rev. Cell Dev. Biol.* *34*, 495–521.
- David, S., and Aguayo, A.J. (1981). Axonal elongation into peripheral nervous system “bridges” after central nervous system injury in adult rats. *Science* *214*, 931–933.
- de Lima, S., Koriyama, Y., Kurimoto, T., Oliveira, J.T., Yin, Y., Li, Y., Gilbert, H.Y., Fagiolini, M., Martinez, A.M., and Benowitz, L. (2012). Full-length axon regeneration in the adult mouse optic nerve and partial recovery of simple visual behaviors. *Proc. Natl. Acad. Sci. USA* *109*, 9149–9154.
- Dobin, A., Davis, C.A., Schlesinger, F., Drenkow, J., Zaleski, C., Jha, S., Batut, P., Chaisson, M., and Gingeras, T.R. (2013). STAR: ultrafast universal RNA-seq aligner. *Bioinformatics* *29*, 15–21.
- Duan, X., Qiao, M., Bei, F., Kim, I.J., He, Z., and Sanes, J.R. (2015). Subtype-specific regeneration of retinal ganglion cells following axotomy: effects of osteopontin and mTOR signaling. *Neuron* *85*, 1244–1256.
- Ertürk, A., Hellal, F., Enes, J., and Bradke, F. (2007). Disorganized microtubules underlie the formation of retraction bulbs and the failure of axonal regeneration. *J. Neurosci.* *27*, 9169–9180.
- Ertürk, A., Becker, K., Jährling, N., Mauch, C.P., Hojer, C.D., Egen, J.G., Hellal, F., Bradke, F., Sheng, M., and Dodt, H.U. (2012). Three-dimensional imaging of solvent-cleared organs using 3DISCO. *Nat. Protoc.* *7*, 1983–1995.
- Fawcett, J.W. (2018). The Paper that Restarted Modern Central Nervous System Axon Regeneration Research. *Trends Neurosci.* *41*, 239–242.
- Geoffroy, C.G., and Zheng, B. (2014). Myelin-associated inhibitors in axonal growth after CNS injury. *Curr. Opin. Neurobiol.* *27*, 31–38.
- Geoffroy, C.G., Hilton, B.J., Tetzlaff, W., and Zheng, B. (2016). Evidence for an Age-Dependent Decline in Axon Regeneration in the Adult Mammalian Central Nervous System. *Cell Rep.* *15*, 238–246.
- Guo, X., Snider, W.D., and Chen, B. (2016). GSK3 β regulates AKT-induced central nervous system axon regeneration via an eIF2B ϵ -dependent, mTORC1-independent pathway. *eLife* *5*, e11903.
- He, Z., and Jin, Y. (2016). Intrinsic Control of Axon Regeneration. *Neuron* *90*, 437–451.
- Hellal, F., Hurtado, A., Ruschel, J., Flynn, K.C., Laskowski, C.J., Umlauf, M., Kapitein, L.C., Strikis, D., Lemmon, V., Bixby, J., et al. (2011). Microtubule stabilization reduces scarring and causes axon regeneration after spinal cord injury. *Science* *331*, 928–931.
- Huang, W., Sherman, B.T., and Lempicki, R.A. (2009a). Bioinformatics enrichment tools: paths toward the comprehensive functional analysis of large gene lists. *Nucleic Acids Res.* *37*, 1–13.
- Huang, W., Sherman, B.T., and Lempicki, R.A. (2009b). Systematic and integrative analysis of large gene lists using DAVID bioinformatics resources. *Nat. Protoc.* *4*, 44–57.
- Hur, E.M., Saijilafu, Lee, B.D., Kim, S.J., Xu, W.L., and Zhou, F.Q. (2011a). GSK3 controls axon growth via CLASP-mediated regulation of growth cone microtubules. *Genes Dev.* *25*, 1968–1981.
- Hur, E.M., Yang, I.H., Kim, D.H., Byun, J., Saijilafu, Xu, W.L., Nicovich, P.R., Cheong, R., Levchenko, A., Thakor, N., and Zhou, F.Q. (2011b). Engineering neuronal growth cones to promote axon regeneration over inhibitory molecules. *Proc. Natl. Acad. Sci. USA* *108*, 5057–5062.
- Hur, E.M., Saijilafu, and Zhou, F.Q. (2012). Growing the growth cone: remodeling the cytoskeleton to promote axon regeneration. *Trends Neurosci.* *35*, 164–174.
- Kim, D., Langmead, B., and Salzberg, S.L. (2015). HISAT: a fast spliced aligner with low memory requirements. *Nat. Methods* *12*, 357–360.
- Kurimoto, T., Yin, Y., Omura, K., Gilbert, H.Y., Kim, D., Cen, L.P., Moko, L., Kügler, S., and Benowitz, L.I. (2010). Long-distance axon regeneration in the mature optic nerve: contributions of oncomodulin, cAMP, and pten gene deletion. *J. Neurosci.* *30*, 15654–15663.
- Lee, J.K., and Zheng, B. (2012). Role of myelin-associated inhibitors in axonal repair after spinal cord injury. *Exp. Neurol.* *235*, 33–42.
- Li, S., Yang, C., Zhang, L., Gao, X., Wang, X., Liu, W., Wang, Y., Jiang, S., Wong, Y.H., Zhang, Y., and Liu, K. (2016). Promoting axon regeneration in the adult CNS by modulation of the melanopsin/GPCR signaling. *Proc. Natl. Acad. Sci. USA* *113*, 1937–1942.
- Lim, J.H., Stafford, B.K., Nguyen, P.L., Lien, B.V., Wang, C., Zukor, K., He, Z., and Huberman, A.D. (2016). Neural activity promotes long-distance, target-specific regeneration of adult retinal axons. *Nat. Neurosci.* *19*, 1073–1084.
- Liu, K., Lu, Y., Lee, J.K., Samara, R., Willenberg, R., Sears-Kraxberger, I., Tedeschi, A., Park, K.K., Jin, D., Cai, B., et al. (2010). PTEN deletion enhances the regenerative ability of adult corticospinal neurons. *Nat. Neurosci.* *13*, 1075–1081.
- Love, M.I., Huber, W., and Anders, S. (2014). Moderated estimation of fold change and dispersion for RNA-seq data with DESeq2. *Genome Biol.* *15*, 550.
- Luo, X., Salgueiro, Y., Beckerman, S.R., Lemmon, V.P., Tsoulfas, P., and Park, K.K. (2013). Three-dimensional evaluation of retinal ganglion cell axon regeneration and pathfinding in whole mouse tissue after injury. *Exp. Neurol.* *247*, 653–662.
- Miao, L., Yang, L., Huang, H., Liang, F., Ling, C., and Hu, Y. (2016). mTORC1 is necessary but mTORC2 and GSK3 β are inhibitory for AKT3-induced axon regeneration in the central nervous system. *eLife* *5*, e14908.
- Moore, D.L., Blackmore, M.G., Hu, Y., Kaestner, K.H., Bixby, J.L., Lemmon, V.P., and Goldberg, J.L. (2009). KLF family members regulate intrinsic axon regeneration ability. *Science* *326*, 298–301.
- Mortazavi, A., Williams, B.A., McCue, K., Schaeffer, L., and Wold, B. (2008). Mapping and quantifying mammalian transcriptomes by RNA-Seq. *Nat. Methods* *5*, 621–628.
- Park, K.K., Liu, K., Hu, Y., Smith, P.D., Wang, C., Cai, B., Xu, B., Connolly, L., Kramvis, I., Sahin, M., and He, Z. (2008). Promoting axon regeneration in the adult CNS by modulation of the PTEN/mTOR pathway. *Science* *322*, 963–966.
- Pernet, V., Joly, S., Jordi, N., Dalkara, D., Guzik-Kornacka, A., Flannery, J.G., and Schwab, M.E. (2013). Misguidance and modulation of axonal regeneration by Stat3 and Rho/ROCK signaling in the transparent optic nerve. *Cell Death Dis.* *4*, e734.
- Pertea, M., Pertea, G.M., Antonescu, C.M., Chang, T.C., Mendell, J.T., and Salzberg, S.L. (2015). StringTie enables improved reconstruction of a transcriptome from RNA-seq reads. *Nat. Biotechnol.* *33*, 290–295.
- Pertea, M., Kim, D., Pertea, G.M., Leek, J.T., and Salzberg, S.L. (2016). Transcript-level expression analysis of RNA-seq experiments with HISAT, StringTie and Ballgown. *Nat. Protoc.* *11*, 1650–1667.
- Pita-Thomas, W., Mahar, M., Joshi, A., Gan, D., and Cavalli, V. (2019). HDAC5 promotes optic nerve regeneration by activating the mTOR pathway. *Exp. Neurol.* *317*, 271–283.
- Richardson, P.M., McGuinness, U.M., and Aguayo, A.J. (1980). Axons from CNS neurons regenerate into PNS grafts. *Nature* *284*, 264–265.
- Robinson, M.D., McCarthy, D.J., and Smyth, G.K. (2010). edgeR: a Bioconductor package for differential expression analysis of digital gene expression data. *Bioinformatics* *26*, 139–140.
- Ruschel, J., Hellal, F., Flynn, K.C., Dupraz, S., Elliott, D.A., Tedeschi, A., Bates, M., Sliwinski, C., Brook, G., Dobrindt, K., et al. (2015). Axonal regeneration. Systemic administration of epothilone B promotes axon regeneration after spinal cord injury. *Science* *348*, 347–352.
- Sekine, Y., Lin-Moore, A., Chenette, D.M., Wang, X., Jiang, Z., Cafferty, W.B., Hammarlund, M., and Strittmatter, S.M. (2018). Functional Genome-wide Screen Identifies Pathways Restricting Central Nervous System Axonal Regeneration. *Cell Rep.* *23*, 415–428.

- Sengottuvel, V., Leibinger, M., Pfreimer, M., Andreadaki, A., and Fischer, D. (2011). Taxol facilitates axon regeneration in the mature CNS. *J. Neurosci.* *31*, 2688–2699.
- Smith, P.D., Sun, F., Park, K.K., Cai, B., Wang, C., Kuwako, K., Martinez-Carrasco, I., Connolly, L., and He, Z. (2009). SOCS3 deletion promotes optic nerve regeneration in vivo. *Neuron* *64*, 617–623.
- So, K.F., and Aguayo, A.J. (1985). Lengthy regrowth of cut axons from ganglion cells after peripheral nerve transplantation into the retina of adult rats. *Brain Res.* *328*, 349–354.
- Sun, F., Park, K.K., Belin, S., Wang, D., Lu, T., Chen, G., Zhang, K., Yeung, C., Feng, G., Yankner, B.A., and He, Z. (2011). Sustained axon regeneration induced by co-deletion of PTEN and SOCS3. *Nature* *480*, 372–375.
- Tanabe, K., Bonilla, I., Winkles, J.A., and Strittmatter, S.M. (2003). Fibroblast growth factor-inducible-14 is induced in axotomized neurons and promotes neurite outgrowth. *J. Neurosci.* *23*, 9675–9686.
- Tedeschi, A., Dupraz, S., Curcio, M., Laskowski, C.J., Schaffran, B., Flynn, K.C., Santos, T.E., Stern, S., Hilton, B.J., Larson, M.J.E., et al. (2019). ADF/Co-filin-Mediated Actin Turnover Promotes Axon Regeneration in the Adult CNS. *Neuron* *103*, 1073–1085.e1076.
- Tsujino, H., Kondo, E., Fukuoka, T., Dai, Y., Tokunaga, A., Miki, K., Yonenobu, K., Ochi, T., and Noguchi, K. (2000). Activating transcription factor 3 (ATF3) induction by axotomy in sensory and motoneurons: A novel neuronal marker of nerve injury. *Mol. Cell. Neurosci.* *15*, 170–182.
- Várkuti, B.H., Képiró, M., Horváth, I.A., Végner, L., Ráti, S., Zsigmond, Á., Hegyi, G., Lenkei, Z., Varga, M., and Málnási-Csizmadia, A. (2016). A highly soluble, non-phototoxic, non-fluorescent blebbistatin derivative. *Sci. Rep.* *6*, 26141.
- Wang, X.W., Li, Q., Liu, C.M., Hall, P.A., Jiang, J.J., Katchis, C.D., Kang, S., Dong, B.C., Li, S., and Zhou, F.Q. (2018). Lin28 Signaling Supports Mammalian PNS and CNS Axon Regeneration. *Cell Rep.* *24*, 2540–2552.e2546.
- Zhang, Y., Williams, P.R., Jacobi, A., Wang, C., Goel, A., Hirano, A.A., Brecha, N.C., Kerschensteiner, D., and He, Z. (2019). Elevating Growth Factor Responsiveness and Axon Regeneration by Modulating Presynaptic Inputs. *Neuron* *103*, 39–51.e35.

STAR★METHODS

KEY RESOURCES TABLE

REAGENT or RESOURCE	SOURCE	IDENTIFIER
Antibodies		
Mouse monoclonal anti- β -actin	Sigma-Aldrich	Cat# A1978; RRID: AB_476692
Mouse monoclonal anti-tubulin β 3 (TUJ1)	Biolegend	Cat# 801202; RRID: AB_10063408
Rabbit polyclonal anti-myosin IIA	Cell Signaling Technology	Cat# 3403; RRID: AB_2147297
Rabbit polyclonal anti-myosin IIB	Biolegend	Cat# 909902; RRID: AB_2749903
Rabbit polyclonal anti-myosin IIB	Thermo Fisher Scientific	Cat# PA5-17026; RRID: AB_11004392
Mouse monoclonal anti-Gapdh	Sigma-Aldrich	Cat# G8795; RRID: AB_1078991
Rabbit monoclonal anti-Cre	Cell Signaling Technology	Cat# 15036; RRID: AB_2798694
Rabbit monoclonal anti-pS6 (Ser235/236)	Cell Signaling Technology	Cat# 4858; RRID: AB_916156
Rabbit monoclonal anti-pAkt (Ser473)	Cell Signaling Technology	Cat# 4060; RRID: AB_2315049
Rabbit monoclonal anti-pGSK3 β (Ser9)	Cell Signaling Technology	Cat# 5558; RRID: AB_10013750
Rabbit monoclonal anti-Atf3	Cell Signaling Technology	Cat# 33593; RRID: AB_2799039
Rabbit monoclonal anti-Gap43	Cell Signaling Technology	Cat# 8945; RRID: AB_10860076
Rabbit monoclonal anti-c-Jun	Cell Signaling Technology	Cat# 9165; RRID: AB_2130165
Rabbit monoclonal anti-c-Myc	Cell Signaling Technology	Cat# 5605; RRID: AB_1903938
HRP-linked goat anti-rabbit IgG	Cell Signaling Technology	Cat# 7074; RRID: AB_2099233
HRP-linked horse anti-mouse IgG	Cell Signaling Technology	Cat# 7076; RRID: AB_330924
Goat anti-mouse IgG (H+L) cross-adsorbed secondary antibody, Alexa Fluor 488	Thermo Fisher Scientific	Cat# A-11001; RRID: AB_2534069
Goat anti-mouse IgG (H+L) cross-adsorbed secondary antibody, Alexa Fluor 568	Thermo Fisher Scientific	Cat# A-11004; RRID: AB_2534072
Goat anti-mouse IgG (H+L) cross-adsorbed secondary antibody, Alexa Fluor 647	Thermo Fisher Scientific	Cat# A-21235; RRID: AB_2535804
Goat anti-rabbit IgG (H+L) cross-adsorbed secondary antibody, Alexa Fluor 488	Thermo Fisher Scientific	Cat# A-11008; RRID: AB_143165
Goat anti-rabbit IgG (H+L) cross-adsorbed secondary antibody, Alexa Fluor 568	Thermo Fisher Scientific	Cat# A-11011; RRID: AB_143157
Purified rat monoclonal anti-mouse CD16/CD32 (mouse Fc block)	BD Biosciences	Cat# 553141; RRID: AB_394656
Rat monoclonal anti-mouse CD90.2 (Thy-1.2), PE	Thermo Fisher Scientific	Cat# 12-0902-81; RRID: AB_465775
Bacterial and Virus Strains		
AAV2-Cre	Signagen Laboratories	Cat# SL100813
AAV2-GFP	Signagen Laboratories	Cat# SL100812
AAV2-Lin28a-FLAG (codon optimized)	Signagen Laboratories	Cat# SL100863
Chemicals, Peptides, and Recombinant Proteins		
Cholera toxin subunit B (recombinant), Alexa Fluor 555 Conjugate	Thermo Fisher Scientific	Cat# C-22843
Tetrahydrofuran	Sigma-Aldrich	Cat# 186562
Benzyl alcohol	Sigma-Aldrich	Cat# 305197
Benzyl benzoate	Sigma-Aldrich	Cat# B6630
Neuron isolation enzyme (with papain)	Thermo Fisher Scientific	Cat# 88285
DNase	Worthington Biochemical Corporation	Cat# LK003170
Fluoroshield	Sigma-Aldrich	F6182
DAPI Fluoromount-G	SouthernBiotech	0100-20

(Continued on next page)

Continued		
REAGENT or RESOURCE	SOURCE	IDENTIFIER
Critical Commercial Assays		
PicoPure RNA isolation kit	Thermo Fisher Scientific	Cat# KIT0204
Deposited Data		
Control and myosin IIA/B knockout RGC RNA-seq	Gene Expression Omnibus	GEO: GSE147328
Control and myosin IIA/B knockout DRG RNA-seq	Gene Expression Omnibus	GEO: GSE147400
Experimental Models: Organisms/Strains		
Myh9 ^{ff} mice	MMRRC	RRID: MMRRC_032096-UNC
Myh10 ^{ff} mice	MMRRC	RRID: MMRRC_016981-UNC
Advillin-Cre	The Jackson Laboratory	RRID: IMSR_JAX:032536
C57Bl6/J mice	The Jackson Laboratory	RRID: IMSR_JAX:000664
tdTomato Cre reporter mice (Ai9)	The Jackson Laboratory	RRID: IMSR_JAX:007909
Recombinant DNA		
pAAV-Ef1a-Lin28a-FLAG (codon optimized)	Wang et al., 2018	N/A
Software and Algorithms		
AxioVision, release 4.8	Zeiss	N/A
Zen	Zeiss	N/A
ImageJ	NIH	N/A
GraphPad Prism 7	GraphPad Software	N/A
STAR, version 2.7.0d	Dobin et al., 2013	N/A
DESeq2, version 1.22.2	Love et al., 2014	N/A
Seqtk	https://github.com/lh3/seqtk	N/A
HISAT2, version 2.0.4	Kim et al., 2015	N/A
StringTie, version 1.3.0	Pertea et al., 2015	N/A
edgeR	Robinson et al., 2010	N/A
DAVID Bioinformatics Resources 6.8	Huang et al., 2009a, 2009b	N/A

RESOURCE AVAILABILITY

Lead Contact

Further information and requests for resources and reagents should be directed to and will be fulfilled by the Lead Contact, Feng-Quan Zhou (fzhou4@jhmi.edu).

Materials Availability

This study did not generate new unique reagents.

Data and Code Availability

The data that support the findings of this study are available from the corresponding author upon reasonable request. RNA-seq raw data and processed data have been deposited to Gene Expression Omnibus (GEO: GSE147328 for RGC RNA-seq, GEO: GSE147400 for DRG RNA-seq).

EXPERIMENTAL MODEL AND SUBJECT DETAILS

Mice

All animal experiments were conducted in accordance with the protocol approved by the Institutional Animal Care and Use Committee of the Johns Hopkins University. The Myh9^{ff} (stock# 032096-UNC) and Myh10^{ff} (stock# 016981-UNC) mouse strains were obtained from Mutant Mouse Resource and Research Center (MMRRC) at University of North Carolina at Chapel Hill, an NIH-funded strain repository, and were donated to the MMRRC by Robert S. Adelstein, M.D., National Heart, Lung, and Blood Institute (NHLBI). The two lines were crossed to generate Myh9^{ff}: Myh10^{ff} mice. Advillin-Cre mouse line (JAX stock# 032536) was a kind gift from Dr. Fan Wang's laboratory at Duke University, and was crossed with Myh9^{ff}: Myh10^{ff} to get Advillin-Cre: Myh9^{ff}: Myh10^{ff} conditional knockout mice. The tdTomato Cre reporter line (Ai9, stock# 007909) was purchased from The Jackson Laboratory. Adult mice (6 weeks) of both sexes were used. Genotypes of the mice were determined by PCR using primers provided by MMRRC and

The Jackson Laboratory. All animal surgeries were performed under anesthesia induced by intraperitoneal injection of ketamine (100 mg/kg) and xylazine (10 mg/kg) diluted in sterile saline. Details of the surgeries are described below.

METHOD DETAILS

Construct

The pAAV-Ef1a-Lin28a-FLAG plasmid was constructed in a previous study (Wang et al., 2018). Briefly, the Lin28a-FLAG open reading frame with a 5' BamHI and a 3' EcoRV restriction sites was synthesized (codon optimized, gBlocks of Integrated DNA Technologies) and used to replace the EYFP open reading frame in pAAV-Ef1a-EYFP, to obtain the pAAV-Ef1a-Lin28a-FLAG plasmid. All restriction enzymes and T4 DNA ligase were purchased from New England Biolabs. Plasmids were amplified using DH5 α competent cells (Thermo Fisher Scientific) and purified with Endofree plasmid maxi kit (QIAGEN).

Optic Nerve Regeneration Model

Intravitreal viral injection, optic nerve crush and RGC axon labeling were performed as previously described (Park et al., 2008). Briefly, under anesthesia, 1.5 μ L of AAV2 virus was injected into the right vitreous humor of a mouse with a Hamilton syringe (32-gauge needle). The position and direction of the injection were well-controlled to avoid injury to the lens. Two weeks later, the right optic nerve of the mouse was exposed intraorbitally and crushed with Dumont #5 fine forceps (Fine Science Tools) for 5 s at approximately 1 mm behind the optic disc. To label RGC axons in the optic nerve, 1.5 μ L of Alexa Fluor 555-conjugated CTB (2 μ g/ μ L, Thermo Fisher Scientific) was injected into the right vitreous humor with a Hamilton syringe (32-gauge needle) 2 days before the mouse was sacrificed by transcardial perfusion under anesthesia. The right optic nerve and bilateral retinas were dissected out and post-fixed in 4% PFA overnight at 4°C. AAV2-Cre (SL100813) was purchased from SignaGen Laboratories. AAV2-Lin28a-FLAG was also packaged by SignaGen Laboratories. All viruses used had titers over 1×10^{13} gc/ml. For post-injury treatment model, all procedures were done in the same way except the intravitreal viral injection was conducted one day after the optic nerve crush.

Optic Nerve Tissue Clearing

Tissue clearing of optic nerves was done based on previous studies (Ertürk et al., 2012; Luo et al., 2013). Briefly, fixed optic nerves were first dehydrated in an ascending serial concentration of tetrahydrofuran (50%, 70%, 80%, 100% and 100%, v/v % in distilled water, 20 min each, Sigma-Aldrich) and then cleared in a solution of benzyl alcohol and benzyl benzoate (BABB, 1:2, Sigma-Aldrich). Incubations were done on an orbital shaker at room temperature. The nerves were stored in BABB in the dark at room temperature.

Analysis of RGC Axon Regeneration

Tissue cleared whole-mount optic nerves were imaged with a 20x objective on a Zeiss LSM 800 confocal microscope. For each optic nerve, Z stack and tiling (10% overlap) functions were used to acquire stacked 2- μ m-thick planes of the whole area of interest and the tiles were stitched. 3D animations were created in Imaris (Bitplane).

To quantify the number of regenerating axons in each optic nerve, every 8 consecutive planes were Z-projected (maximum intensity) to generate a series of Z-projection images of 16- μ m-thick optical sections. At each 250- μ m interval from the crush site, the number of CTB-labeled axons was counted in each Z-projection image and summed over all optical sections.

To quantify the average length of top 5 longest axons of each optic nerve, all stitched 2- μ m-thick planes were Z-projected (maximum intensity) to obtain a single Z-projection image of the nerve. Top 5 longest regenerating axons were manually traced from the axonal tips to the crush site using the Fiji software (NIH) to acquire the lengths of the axons.

Immunohistochemistry of Whole-Mount Retinas

Fixed retinas were first radially cut into a petal shape (4 incisions) and blocked with PBST (1%) containing 10% goat serum for 1 hr at room temperature. The retinas were then sequentially stained with primary antibodies overnight at 4°C, and corresponding Alexa Fluor-conjugated secondary antibodies (1:500, Thermo Fisher Scientific) for 2 hr at room temperature. All antibodies were diluted with the blocking buffer. Following each antibody incubation, the retinas were washed with PBST (0.3%) for 4 times (15 min each). After the last wash, the retinas were mounted onto slides with Fluoroshield (Sigma-Aldrich). Fluorescent images of the flat-mounted retinas were acquired with a 20x objective on a Zeiss LSM 800 confocal microscope.

Analysis of RGC Transduction Rate

To quantify RGC transduction rate, uninjured right retinas (without optic nerve crush) were taken from transcardially perfused *Myh9^{fl/fl}*:*Myh10^{fl/fl}* mice 2 weeks after intravitreal AAV2-Cre injection. The retinas were stained with mouse anti-tubulin β 3 (Tuj1, 1:500, BioLegend) and rabbit anti-Cre recombinase (1:100, Cell Signaling Technology) antibodies following the steps mentioned above (see Immunohistochemistry of whole-mount retinas). Five to eight fields under 20x objective were randomly obtained from the peripheral regions of each flat-mounted retina. For each mouse, RGC transduction rate was calculated by dividing the total number of Cre⁺/Tuj1⁺ cells in all fields by the total number of Tuj1⁺ cells in all fields. Only cells in the ganglion cell layer were counted.

Analysis of RGC Survival Rate

To quantify RGC survival rate, C57Bl6/J and *Myh9^{ff}: Myh10^{ff}* mice injected with AAV2-Cre were transcardially perfused 2 weeks after optic nerve crush and both retinas of each mouse were collected. The retinas were stained with mouse anti-tubulin β 3 antibody (Tuj1, 1:500, BioLegend) following the steps mentioned above (see [Immunohistochemistry of whole-mount retinas](#)). Seven or eight fields under 20x objective were randomly taken from the peripheral regions of each flat-mounted retina. For each mouse, RGC survival rate was calculated by dividing the average number of Tuj1⁺ cells in one field in the injured retina (right) by that in the uninjured retina (left). Only cells in the ganglion cell layer were counted.

Immunohistochemistry of Retinal Sections

Fixed retinas were sectioned with a cryostat (10 μ m) and the retinal sections were warmed on a slide warmer at 37°C for 1 hr. Sections were rinsed once in PBS, soaked in 100°C citrate buffer (pH 6) for 15 min, let to cool in the buffer to room temperature and then washed twice (5 min each) in PBS. After being blocked with PBST (0.3%) containing 10% goat serum at room temperature for 1 hr, the sections were stained with primary antibodies against target molecules overnight at 4 °C, followed by corresponding Alexa Fluor-conjugated secondary antibodies (1:500, Thermo Fisher Scientific) at room temperature for 1 hr. All antibodies were diluted with the blocking buffer. The sections were washed for 4 times (5, 5, 10, 10 min) with PBST (0.3%) following each antibody incubation and finally mounted with DAPI Fluoromount-G (SouthernBiotech). Fluorescent images of the retinal sections were taken with a CCD camera connected to a Zeiss inverted fluorescence microscope controlled by AxioVision software.

Analysis of Myosin IIB Level in RGCs

To analyze myosin IIB level in RGCs, both retinas (uninjured, left side naive, right side injected) of each mouse were taken from transcardially perfused *Myh9^{ff}: Myh10^{ff}* mice 2 weeks after intravitreal AAV2-Cre injection and sectioned. The retinal sections were stained with mouse anti-tubulin β 3 (Tuj1, 1:500, BioLegend) and rabbit anti-myosin IIB (1:100, Thermo Fisher Scientific) antibodies following the steps mentioned above (see [Immunohistochemistry of retinal sections](#)).

To quantify the fluorescence intensity of myosin IIB in all RGCs, at least 7 non-adjacent retinal sections acquired with identical imaging configurations were analyzed for each retina. Fluorescence intensity was measured using the “outline spline” function of AxioVision and the background fluorescence intensity was subtracted.

Analysis of S6 and GSK3 β Phosphorylation

To analyze S6 and GSK3 β phosphorylation in RGCs, C57Bl6/J and *Myh9^{ff}: Myh10^{ff}* mice injected with AAV2-Cre, and *Myh9^{ff}: Myh10^{ff}* mice injected with AAV2-Lin28a-FLAG were transcardially perfused 2 weeks after optic nerve crush and the right retina of each mouse was collected and sectioned. The retinal sections were stained with mouse anti-tubulin β 3 antibody (Tuj1, 1:500, BioLegend), and rabbit anti-pS6 Ser235/236 (1:200, Cell Signaling Technology) or rabbit anti-pGSK3 β Ser9 (1:200, Cell Signaling Technology) antibody following the steps mentioned above (see [Immunohistochemistry of retinal sections](#)).

To quantify the percentage of pS6⁺ or pGSK3 β ⁺ RGCs, at least 363 or 434 RGCs from at least 7 non-adjacent retinal sections from each mouse were analyzed. For each mouse, the percentage of pS6⁺ or pGSK3 β ⁺ RGCs was calculated by dividing the number of pS6⁺/Tuj1⁺ or pGSK3 β ⁺/Tuj1⁺ cells by the number of Tuj1⁺ cells. Only cells in the ganglion cell layer were counted.

The relative fluorescence intensity of each RGC was calculated by dividing the fluorescence intensity of the RGC by that of its adjacent tissue. To quantify the fluorescence intensity of pS6 or pGSK3 β in all RGCs, 20 retinal sections acquired with identical imaging configurations from at least 2 mice were analyzed for each group. To quantify the fluorescence intensity of pS6 or pGSK3 β in S6-activated or GSK3 β -inactivated RGCs, at least 40 RGCs with identical imaging configurations from at least 2 mice were analyzed for each group. Fluorescence intensity of RGCs were measured using the “outline spline” function of AxioVision.

Sciatic Nerve Injury Model

Under anesthesia, bilateral sciatic nerves of a mouse were exposed and transected with spring scissors right below pelvis. Nerves were only exposed but not transected in a sham surgery. Three days after the surgery, the mouse was euthanized and bilateral L4/5 DRGs were collected and used for total RNA or protein extraction.

RGC Purification

Retinas were dissected and digested with papain (Thermo Fisher Scientific) containing 0.005% DNase (Worthington) at 37°C for 8 min. After enzymatic digestion, the retinas were triturated into cell suspension with NeuroBasal medium containing 1% BSA, and the cell suspension was filtered through a 40- μ m cell strainer. The cells were pelleted by centrifugation at 500 g for 5 min, and resuspended in NeuroBasal medium containing 1% BSA. The cells were first blocked with mouse CD16/CD32 Fc block antibody (1:50) for 5 min on ice, and then labeled with PE-conjugated anti-CD90.2 antibody (1:100) for 30 min on ice. After that, the cells were washed twice with HBSS containing 1% BSA, pelleted by centrifugation at 500 g for 5 min, and again resuspended in Neurobasal medium containing 1% BSA. Propidium iodide (PI) was added into the cell suspension and mixed to label the dead cells 2 min before the cells were loaded into the cell sorter. CD90.2 positive/PI negative cells were identified on a Beckman Coulter MoFlo Legacy Cell Sorter and sorted into NeuroBasal medium containing 1% BSA with a 100- μ m nozzle. For each biological replicate in western blot and RNA-seq, 3 retinas from 3 different mice were combined.

RGC RNA Sequencing and Data Analysis

Total RNA of RGCs purified by FACS was isolated using the PicoPure RNA isolation kit (Thermo Fisher Scientific) following the manufacturer's manual and RNA quality was verified using Agilent fragment analyzer (Agilent Technologies). RNA libraries were prepared using the TruSeq stranded total RNA kit (Illumina) following the manufacturer's recommended procedure and QC'ed by Agilent fragment analyzer. Libraries were quantitated using both Qubit (Thermo Fisher Scientific) and Kappa library quantification kit (Roche). The final pooled libraries were sequenced on NextSeq 500 using High Output kit (Illumina) for 2 × 75 paired reads, resulting in at least 80 million reads per library.

Raw FASTQ data were mapped to mouse reference genome (GRCm38) using STAR aligner (version 2.7.0d) (Dobin et al., 2013) with default parameters. The number of counts per gene was estimated using the "quantMode" command in STAR. Quantified raw counts were used in DESeq2 (version 1.22.2) (Love et al., 2014) for the analysis of differentially expressed genes (DEGs). Genes with less than 50 counts in total from six libraries were excluded from analysis. Genes with adjusted $p < 0.05$ and \log_2 fold change > 1 were chosen as DEGs. Principle component analysis and sample similarity were also performed with the transformed count matrix in DESeq2. Normalized counts were used to produce scatterplots and calculate Pearson correlations between pairwise libraries. GO analysis (biological process) was done using DAVID Bioinformatics Resources 6.8 (Huang et al., 2009a, 2009b).

DRG mRNA Sequencing and Data Analysis

Total RNA was isolated with RNeasy mini kit (QIAGEN) and RNA integrity was determined by Agilent 2100 bioanalyzer and RNA 6000 Nano kit (Agilent Technologies). Paired-end libraries were synthesized using the TruSeq RNA library preparation kit (Illumina). Purified libraries were quantified by Qubit 2.0 fluorometer (Thermo Fisher Scientific) and validated by Agilent 2100 bioanalyzer (Agilent Technologies) to confirm the insert size and calculate the mole concentration. Cluster was generated by cBot with the library diluted to 10 pM and sequencing was done on HiSeq 2500 (Illumina).

Sequencing raw reads were preprocessed by filtering out rRNA reads, sequencing adapters, short-fragment reads and other low-quality reads using Seqtk (<https://github.com/lh3/seqtk>). HISAT2 (version 2.0.4) (Kim et al., 2015) was used to map the cleaned reads to the mouse GRCm38.p4 (mm10) reference genome with two mismatches. After genome mapping, StringTie (version 1.3.0) (Pertea et al., 2015, 2016) was run with a reference annotation to generate FPKM values for known gene models (Mortazavi et al., 2008). Differentially expressed genes were identified using edgeR (Robinson et al., 2010). The P value significance threshold in multiple tests was set by the false discovery rate (FDR) (Benjamini and Hochberg, 1995; Benjamini and Yekutieli, 2001). The cut-off for differentially expressed genes was set as $p < 0.05$ and \log_2 fold change > 1 . GO analysis (biological process) was done using DAVID Bioinformatics Resources 6.8 (Huang et al., 2009a, 2009b).

Western Blot Analysis

Total protein was extracted from L4/5 DRGs or purified RGCs using the RIPA buffer (Sigma-Aldrich) containing protease inhibitor cocktail (Sigma-Aldrich) and phosphatase inhibitor cocktail (Sigma-Aldrich). Identical amount of total protein from each condition was then separated by 4%–12% gradient SDS-PAGE gel electrophoresis and transferred onto polyvinylidene fluoride membranes. After being blocked with TBST (1%) containing 5% blotting-grade blocker (Bio-Rad), the membranes were incubated overnight with primary antibodies against target molecules at 4 °C, followed by corresponding HRP-linked secondary antibodies (1:2000, Cell Signaling Technology) for 1 hr at room temperature. All antibodies were diluted with blocking buffer. The membranes were washed with TBST (1%) for four times (5, 5, 10, 10 min) after each antibody incubation. Rabbit primary antibodies against myosin IIA (1:1000), Atf3 (1:1000), Gap43 (1:1000), c-Jun (1:1000), c-Myc (1:1000), pAkt Ser473 (1:2000), pGSK3 β Ser9 (1:1000), pS6 Ser235/236 (1:2000) were purchased from Cell Signaling Technology. Rabbit anti-myosin IIB primary antibody (1:1000) was obtained from Biologend. Mouse anti- β -actin (1:5000) and anti-Gapdh (1:10000) primary antibodies were from Sigma-Aldrich.

Analysis of Axonal Tip Morphology

The method was derived from a previous study (Ertürk et al., 2007). For each optic nerve, top 10 longest axons were first identified in the Z-projection image of the nerve. Then the maximum diameter of each axonal tip and the diameter of the cylindrical shaft of the corresponding axon were measured using Fiji software (NIH), and a tip/shaft ratio was calculated. An axonal tip was defined as a retraction bulb if its tip/shaft ratio was over 4. Otherwise, it was defined as a growth cone.

Analysis of Axon Extension Efficiency

For each optic nerve, a 250- μ m-long region with equivalent number of axons in the Z-projection image of the nerve was used for analysis. All traceable axons within this region were manually traced. For each axon, the length (covered distance on its trajectory) and the displacement (distance along the longitudinal axis of the nerve, could be zero or negative sometimes) between the start point and the end point were measured using Fiji software (NIH). The extension efficiency of each nerve was calculated by dividing the summed displacement by the summed length of all axons.

Analysis of U-turn Rate

For each optic nerve, top 15 longest axons were first identified in the Z-projection image of the nerve and then their trajectories near the axonal tips were traced. A U-turn was defined when the angle between the final direction of the axonal tip and the positive

longitudinal axis of the optic nerve was larger than 90 degrees. The U-turn rate of each nerve was calculated by dividing the number of axons that made U-turns by 15.

QUANTIFICATION AND STATISTICAL ANALYSIS

Statistical analyses were done with GraphPad Prism 7 and the significance level was set as $p < 0.05$. Data are represented as mean \pm SEM unless specifically stated. For comparisons between two groups, two-tailed unpaired or paired t test was used. For comparisons among three or more groups, one-way ANOVA followed by Tukey's multiple comparisons test was used to determine the statistical significance. Fisher's exact test was used to test contingency tables. All details regarding statistical analyses, including the tests used, *P values*, exact values of *n*, definitions of *n*, are described in figure legends.